Eindhoven University of Technology

Eindhoven University of Technology

MASTER

High pressure nucleation of alkanes

Jonkers, P.G.

*Award date:*
2005

Link to publication

**TU/e** technische universiteit eindhoven

Faculteit Technische
Natuurkunde
Groep Gasdynamica
Gebouw Cascade
Postbus 513
5600 MB Eindhoven

| | |
|---|---|
| Titel: | **High Pressure Nucleation of Alkanes** |
| Auteur: | P.G. Jonkers |
| Verslagnummer: | R-1682-A |
| Datum: | September, 2005 |

Vakgroep : Gas Dynamics, Department of Applied Physics,
Eindhoven University of Technology, The Netherlands
Begeleiders : ir. D.G. Labetski
prof. dr. ir. M.E.H. van Dongen

# Contents

# Abstract

Knowledge about condensation of alkanes at high pressures is important for natural gas industry. In this report some aspects of the condensation phenomena in the alkane mixtures are studied.

Classical unary nucleation theory is compared to a binary nucleation model for the case of nonane nucleation in a methane carrier gas at high pressures. Results from numerical calculations show no significant difference between the unary classical theory and the binary nucleation model, and makes the use of unary theory at this point preferable because of its simplicity. At pressures below approximately $25bar$, both theories predict the trend as observed in experiments. At higher pressures, both theories fail to predict the trend of the experiments. This probably has to do with the model for the cluster the surface energy, which fails at high pressures.

Nucleation rates and droplet growth rates are determined by applying the pulse-expansion wave tube in combination with light scattering and light extinction. Experimental results are shown for the ternary methane-propane-nonane mixture at a nucleation temperature of $235K$ and $10bar$. The propane vapour fraction was close to 1%. Droplet growth results are used in order to reduce the scatter in the nonane vapour fraction and so reduce scatter in nucleation rates. Experiments show no significant influence of propane on the nucleation process, which is in agreement with the theoretical predictions.

# Acknowledgements

I would like to thank all the people who were involved in this project. First of all my supervisor ir. D.G. Labetski for all his time, effort and patience. He helped me understand the difficult theory and came up with good ideas that aided me during my project. I'd also like to thank prof. dr. ir. M.E.H. van Dongen for his supervision and critical point of view on most of the theoretical work. Finally my thanks goes to the rest of the "nucleation group" which helped create a good atmosphere to work in. The weekly meetings certainly helped me to focus on all aspects of the project.

Eindhoven, September 2005
Peter Jonkers

# Chapter 1

# Introduction

## 1.1  Background

Many environmental and technological processes deal with phase transitions. An important class of phase transitions is that from the vapour to liquid state, called condensation. Homogeneous condensation is the vapour to liquid transition in the absence of foreign particles. The first stage of homogeneous condensation is the nucleation process. During this stage several tens to hundreds of molecules form a stable cluster (critical cluster), which can grow further to a macroscopic droplet. The latter process is called droplet growth and differs essentially from nucleation.

In this report the nucleation behaviour and droplet growth of supersaturated nonane in methane carrier gas and a methane-propane carrier gas mixture are studied. The idea of studying these systems comes from new developments in natural gas industry. The controlled generation of nucleation and droplet growth in newly developed gas/vapour separators has been shown to be possible. Natural gas contains mainly methane and numerous other components like propane, pentane, nonane etc., carbon dioxide and water. The phase behaviour of natural gas is determined to a large extent by the heavier hydrocarbons. When the gas mixture is brought into a supersaturated state, homogeneous nucleation may take place. Before the natural gas is delivered to the customers, a large part of these condensable components has to be removed. This is achieved with the newly developed gas/vapour separator in the following way. First the gas is accelerated to a supersonic speed by a nozzle. Because of the isentropic acceleration the temperature and pressure of the gass will drop, creating supersaturation of vapour components in the gas mixture. Nucleation will take place and droplets begin to grow. Subsequently, a vortex is induced in the gas flow by means of a vortex generator. The droplets in the flow will be swirled to the outside of the tube. As a result the core of the flow will become dry, while the outside of the flow will contain most of the vapour components. The outer layer of the flow is then separated

1

from the core of the flow, leaving only the dry gas in the flow. In order to increase the performance of the separators, a good understanding of all the processes is needed. This report treats nucleation of alkane mixtures from both a theoretical and an experimental point of view [1][2][3].

## 1.2   Overview

The report starts with a theoretical treatment of nucleation theory, nucleation kinetics, unary and binary nucleation models are discussed.

The second chapter is about diffusion controlled droplet growth. Using the mass balance of a growing droplet, a final expression will be derived which is used to analyse experimental results on droplet growth. The Wilke and Lee method for calculating diffusion coefficients is discussed.

The experimental procedure for performing nucleation experiments is discussed in chapter 4. Nucleation experiments are performed using a modified expansion wave tube, creating a desired saturation time history suitable for studying nucleation and droplet growth. Mixture preparation and droplet detection are outlined.

In chapter 5, equilibrium models are presented for several mixtures. These models form an engineering tool for calculating phase equilibria. All models are based on the RKS equation of state, and were constructed using the PE2000 software for a range of conditions. The equilibrium models are also compared to experimental data.

The following chapter presents numerical calculations of nucleation rates of supersaturated nonane in methane carrier gas, using the binary nucleation model developed in chapter 2. Non-idealities of the gas mixture are discussed and incorporated in the model. Models for calculation of the surface tension are discussed. Numerical results are compared to the classical unary theory and experimental results.

Chapter 7 presents results from nucleation experiments performed with a methane-propane-nonane mixture. The influence of propane on the nucleation process is examined.

The report ends with the main conclusions and some recommendations for future work.

# Chapter 2

# Nucleation Theory

## 2.1 Unary Nucleation Theory

This section on unary nucleation theory follows the approach as described by Luijten [1]. At some points this theory is extended.

### 2.1.1 Unary Nucleation Kinetics

A cluster consisting of $n_v$ molecules can grow by collisions with clusters of any size. It can shrink by evaporation of clusters smaller than itself. As normally is done, the description of cluster formation is limited to the case of impingement and loss only of single molecules (monomers). The kinetic process of nucleation can under this assumption be depicted as in Fig. 2.1. There is a net "flow" rate of clusters in size space from size $n_v$ to size $n_v + 1$. This
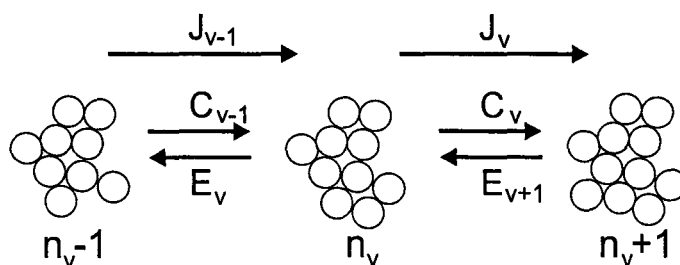


Figure 2.1: *Schematic picture of unary nucleation kinetics. $C_v$ and $E_v$ are condensation and evaporation rates, $J_v$ is the net transition from $n_v$ to $n_v + 1$.*

net flow rate (in number per cubic meter per second) is the result of catching a molecule by a $n_v$-cluster (condensation) and the spontaneous loss of a molecule by a $n_v + 1$-cluster (evaporation).

$$J_v = C_v \rho_v - E_{v+1} \rho_{v+1}, \tag{2.1}$$

3

The condensation rate $C_v$ is the product of the surface area of the $n_v$-cluster, the impingement rate of monomers and the sticking probability (which is commonly set to unity). So the condensation rate can be described by

$$C_v = a_0 n_v^{2/3} \rho_1 \left( \frac{k_B T}{2\pi m_v} \right)^{1/2},  \tag{2.2}$$

where $m_v$ is the mass of a vapour molecule and $a_0$ is a molecular surface area. For a spherical cluster (with $v_v^l = V_v^l / n_v$) it is equal to

$$a_0 = (36\pi)^{1/3} (v_v^l)^{2/3}.  \tag{2.3}$$

The rate of change of the number density of $n_v$-clusters $\rho_v$ is given by

$$\frac{d\rho_v}{dt} = J_{v-1} - J_v,  \tag{2.4}$$

There are two limiting cases that result in vanishing of the time derivative in Eq. (2.1). In equilibrium $d\rho_v^{eq}/dt = 0$ as $J_v = 0$ for all $n_v$. This is called the detailed balance condition where

$$C_v^{eq} \rho_v^{eq} = E_{v+1}^{eq} \rho_{v+1}^{eq}.  \tag{2.5}$$

The second possibility is steady-state nucleation where $J_v = J$ for all $n_v$. It is assumed that the evaporation rate only depends on temperature $T$ and cluster size $n_v$ and not on the vapour content of the surroundings, so $E_{v+1} = E_{v+1}^{eq}$, which gives for the nucleation rate, using Eqs. (2.1) and (2.5)

$$\frac{J}{C_v^{eq} \rho_v^{eq}} = \frac{C_v \rho_v}{C_v^{eq} \rho_v^{eq}} - \frac{\rho_{v+1}}{\rho_{v+1}^{eq}}.  \tag{2.6}$$

As $C_v$ is proportional to the monomer density, $C_v/C_v^{eq} = S$, given that the vapour consists mainly of monomers. Dividing both sides of Eq. (2.6) by $S^{n_v+1}$ yields

$$\frac{J}{C_v \rho_v^{eq} S^{n_v}} = \frac{\rho_v}{\rho_v^{eq} S^{n_v}} - \frac{\rho_{v+1}}{\rho_{v+1}^{eq} S^{n_v+1}}.  \tag{2.7}$$

This equation can be summed from $n_v = 1$ to $N_v$, which results in

$$J \sum_{n_v=1}^{N_v} \left( \frac{1}{C_v \rho_v^{eq} S^{n_v}} \right) = 1 - \frac{\rho_{N_v+1}}{\rho_{N_v+1}^{eq} S^{N_v+1}}.  \tag{2.8}$$

The last term vanishes for sufficiently large $N_v$. Which gives

$$J = \left[ \sum_{n_v=1}^{\infty} \frac{1}{C_v \rho_v^{eq} S^{n_v}} \right]^{-1}.  \tag{2.9}$$

The sum can be replaced by an integral giving

$$J = \left[ \int_1^{\infty} \frac{1}{C_v \rho_v^{eq} S^{n_v}} dn_v \right]^{-1}.  \tag{2.10}$$

### 2.1.2  Unary Nucleation Theory

The number density of $n_v$-clusters is governed by a Boltzmann law:

$$\rho_v \propto \exp\left(-\frac{\Delta G_v}{k_B T}\right) \qquad (2.11)$$

where $\Delta G_v$ is the free energy of formation of a cluster consisting of $n_v$ molecules. From thermodynamical considerations the free energy of formation in phase equilibrium is given by,

$$\Delta G_v^{eq} = \sigma a_0 n_v^{2/3}, \qquad (2.12)$$

where $\sigma$ is the surface tension of the liquid phase. This results in the equilibrium number density of $n_v$-clusters in the equilibrium state,

$$\rho_v^{eq} = \rho_1^{eq} \exp\left(-\frac{\Delta G_v^{eq}}{k_B T}\right) = \rho_1^{eq} \exp(-\theta n_v^{2/3}). \qquad (2.13)$$

Here $\theta$ is the dimensionless surface tension, which is defined as

$$\theta = \frac{\sigma a_0}{k_B T}. \qquad (2.14)$$

For clusters in the supersaturated state the formation energy is

$$\Delta G_v = -n_v k_B T \ln S + \sigma a_0 n_v^{2/3}, \qquad (2.15)$$

which results in a cluster distribution given by

$$\rho_v = \rho_1 \exp\left(-\frac{\Delta G_v}{k_B T}\right) = \rho_1 \exp(n_v \ln S - \theta n_v^{2/3}). \qquad (2.16)$$

Fig. 2.2 shows the behaviour of the cluster formation energy for different values of supersaturation. For a supersaturated vapour there will be a maximum at some critical cluster-size value $n_v^*$. Clusters smaller than $n_v^*$ will tend to evaporate, whereas clusters larger than $n_v^*$ have a good chance to become stable and grow further. The critical cluster-size can be calculated with $(\partial \Delta G_v / \partial n_v) = 0$ for $n_v^*$, resulting in

$$n_v^* = \left(\frac{2\theta}{3 \ln S}\right)^3. \qquad (2.17)$$

The corresponding value of the formation energy for the critical cluster is equal to

$$\frac{\Delta G_v^*}{k_B T} = \frac{4}{27} \frac{\theta^3}{(\ln S)^2}. \qquad (2.18)$$

The combination $S^{n_v} \rho_v^{eq}$ in the denominator of the integral expression of the nucleation rate Eq. (2.10) can be written as

$$S^{n_v} \rho_v^{eq} = \rho_1^{eq} \exp(n_v \ln S - \theta n_v^{2/3}) = \rho_1^{eq} \exp\left(-\frac{\Delta G_v}{k_B T}\right). \qquad (2.19)$$
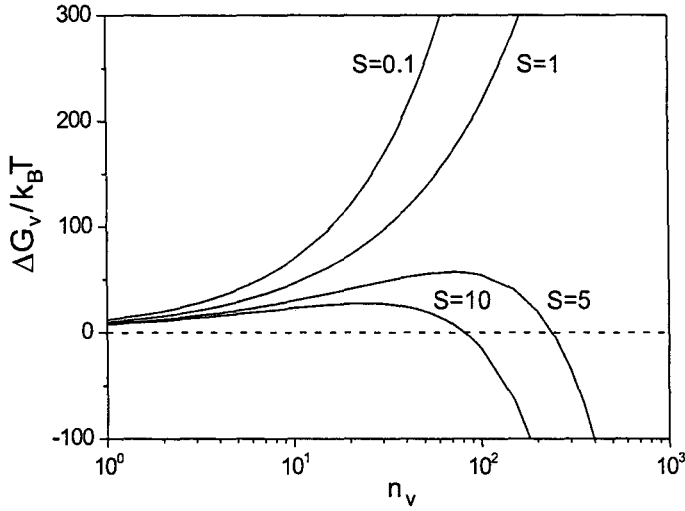
Figure 2.2: *Free energy of cluster formation versus number of molecules in the cluster, for different values of supersaturation S (theta=10).*

As the exponents exhibits a sharp minimum at the critical size, the only significant contributions to the integral can come from the region near $n_v^*$. Therefore the energy of formation is expanded into a second order Taylor series near $n_v^*$:

$$\Delta G_v \simeq \Delta G_v^* - \zeta^2 \pi k_B T (n_v - n_v^*)^2, \tag{2.20}$$

with the Zeldovich factor $\zeta$ given by

$$\zeta = \left[ \frac{-1}{2\pi k_B T} \left( \frac{\partial^2 \Delta G_v}{\partial n_v^2} \right)_{n_v = n_v*} \right]^{1/2} = \frac{1}{3} \left( \frac{\theta}{\pi} \right)^{1/2} (n_v^*)^{-2/3}. \tag{2.21}$$

The collision rate $C_v$ varies much more slowly with $n_v$ as $\rho_v^{eq} S^{n_v}$ and can therefore be put in front of the integral as $C_v^*$. Substituting Eqs. (2.19) and (2.20) into (2.10) gives

$$J = C_v^* \rho_1^{eq} \exp \left( -\frac{\Delta G_v^*}{k_B T} \right) \left[ \int_1^\infty \exp[-\zeta^2 \pi (n_v - n_v^*)^2] dn_v \right]^{-1}. \tag{2.22}$$

When the integration interval is extended from $-\infty$ to $\infty$, the remaining integral is of Gaussian type. The evaluation is standard and yields $\zeta^{-1}$. The final expression for $J$ is arrived at by substitution of Eqs. (2.2), (2.18) and (2.21) giving

$$J = \rho_1 \rho_1^{eq} v_v^l \left( \frac{2\sigma}{\pi m_v} \right)^{1/2} \exp \left[ -\frac{4}{27} \frac{\theta^3}{(\ln S)^2} \right]. \tag{2.23}$$

This is the result of the classical nucleation theory. There is a problem with this result concerning so-called limiting consistency. Inspection of Eq. (2.12) shows that the formation energy of monomers is not zero, which it should be in a consistent model. The most widely used correction is to replace Eq. (2.12) by

$$\frac{\Delta G_v^{eq}}{k_B T} = \theta(n^{2/3} - 1),\tag{2.24}$$

which leads to a correction factor $e^\theta$ in the nucleation rate $J$. The final result of this so-called *internally consistent classical theory* (ICCT) is

$$J = \rho_1 \rho_1^{eq} v_v^l \left(\frac{2\sigma}{\pi m_v}\right)^{1/2} \exp\left[\theta - \frac{4}{27}\frac{\theta^3}{(\ln S)^2}\right].\tag{2.25}$$

### 2.1.3 Theoretical Considerations

In the derivation to classical unary theory one of the steps was to make a second order Taylor expansion of the cluster formation energy. Subsequently the integral was extended from $-\infty$ to $\infty$ in order to arrive at an integral of Gaussian type. The question for what values of $\theta$ and $S$ the approximation of the nucleation integral Eq. (2.10) as the Gaussian type integral Eq. (2.22) is justified. This effect was studied by looking at the integrand of the nucleation rate, $(C_v \rho_v^{eq} S^{n_v})^{-1}$ and dismissing all the pre-factors. This results in

$$f(n_v) = \frac{1}{n_v^{2/3} \exp(n_v \ln S - \theta n^{2/3})}.\tag{2.26}$$

For the Gaussian type integral of the classical theory we find

$$f_{Gauss}(n_v) = \frac{1}{(n_v^*)^{2/3} \exp(n_v^* \ln S - \theta(n^*)^{2/3})} \exp\left[-\frac{1}{9}\frac{\theta}{(n_v^*)^{4/3}}(n_v - n_v^*)^2\right].\tag{2.27}$$

Eq. (2.26) is the exact discrete expression of the integrand, where Eq. (2.27) is the approximated continuous expression. Fig. 2.3 shows these functions for two situations with different values for $S$ and $\theta$. As can be seen, the approximated Gauss-function fits very well for large critical clusters. For a very small critical cluster-size however, the Gauss-function does not give an accurate description. Moreover the Gauss-function is also evaluated for negative $n_v$-values. In order to evaluate the effect of this Gaussian approximation on the nucleation rate one has to compare the Gaussian nucleation integrand

$$\bar{J}_{Gauss} = \left[\int_{-\infty}^{\infty} f_{Gauss}(n_v) dn_v\right]^{-1},\tag{2.28}$$

with the discrete nucleation sum

$$\bar{J} = \left[\sum_{n_v=1}^{\infty} f(n_v)\right]^{-1}.\tag{2.29}$$

(a)                                                      (b)
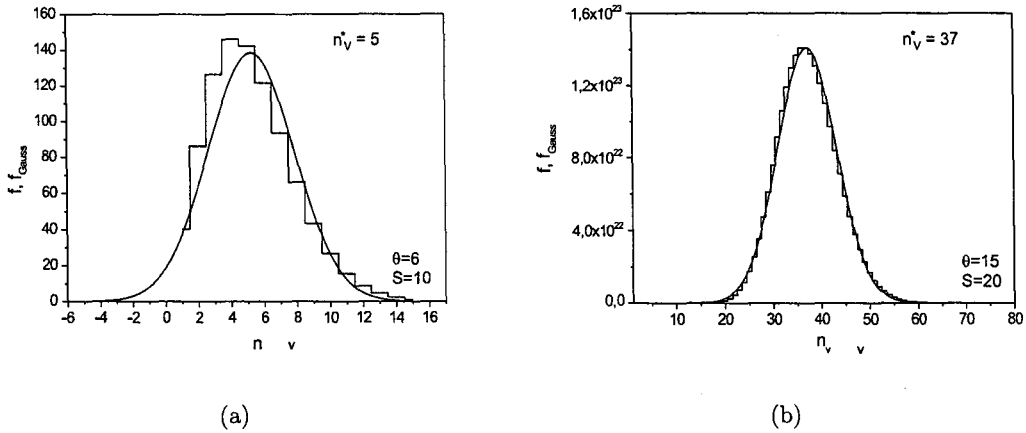
Figure 2.3: *Comparison of continuous Gauss profile ($f_{Gauss}(n_v)$) and discrete profile ($f(n_v)$) for (a) $\theta = 6$, $S = 10$ (b) $\theta = 15$, $S = 20$.*

The approximation error $\delta$ is given by

$$\delta = \frac{\bar{J} - \bar{J}_{Gauss}}{\bar{J}}, \qquad (2.30)$$

which were evaluated for different values of $S$ and $\theta$. In Fig. 2.4 the approximation error is plotted against $S$ for several values of $\theta$. The dashed line in the plots is the maximum supersaturation for given $\theta$, belonging to a critical cluster-size of three. One can see that the approximation error is no larger than about 2%, and decreases rapidly to very small values with decreasing $S$. We conclude that using the Gaussian approximation to calculate the nucleation integral Eq. (2.10) is justified. The errors in the nucleation rates caused by the approximation are negligible for the studied range of $S$ and $\theta$ parameters.

## 2.2  A Binary Nucleation Model for a Dilute Vapour in a Carrier Gas

In this section we consider nucleation of a dilute supersaturated vapour in a subsaturated active carrier gas. The carrier gas does not nucleate itself but enters the clusters for entropic reasons only.

### 2.2.1  Binary Nucleation Kinetics

Binary nucleation kinetics can be treated in a similar fashion as in the unary case. A cluster consisting of $n_v$ vapour and $n_g$ gas molecules can grow by collisions with clusters of any
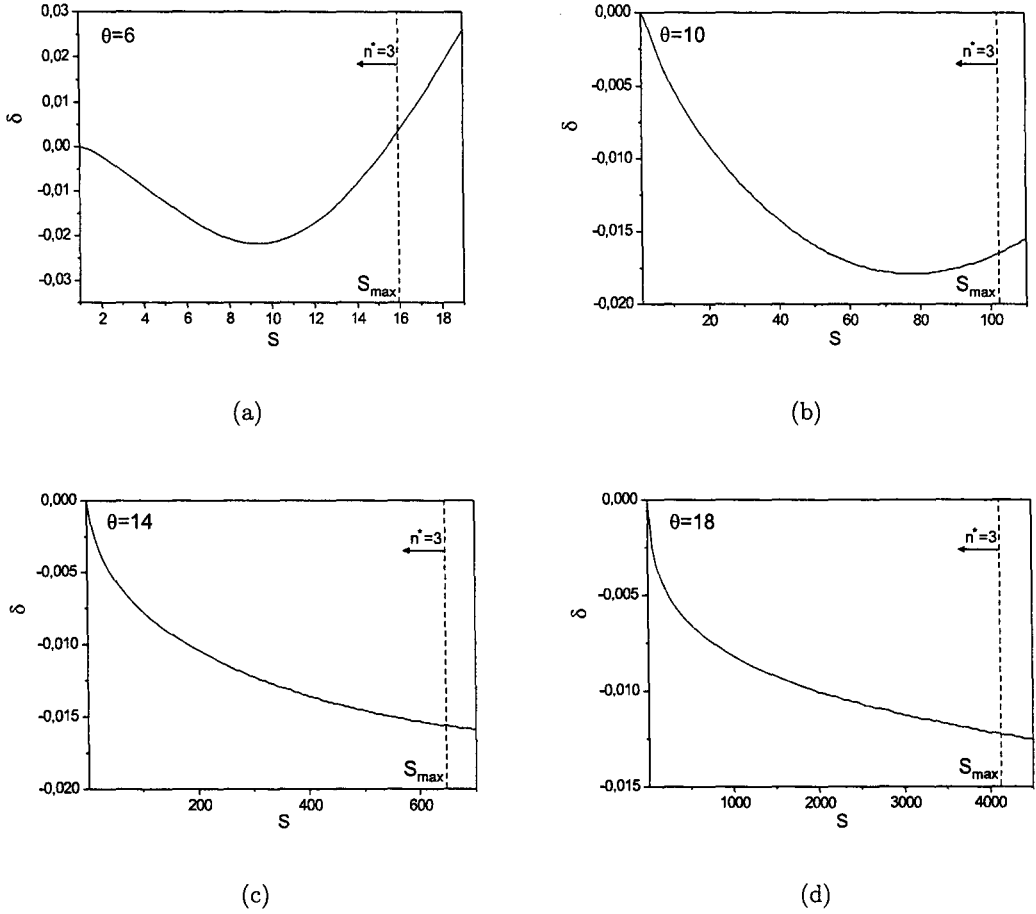
Figure 2.4: *Approximation error of Gaussian classical nucleation rate as function of S for (a) $\theta = 6$ (b) $\theta = 10$ (c) $\theta = 14$ (d) $\theta = 18$.*

size and shrink by emission of clusters of smaller size. Again the description is limited to the case of impingement and loss of vapour or gas monomers. The kinetic process of nucleation kinetics can be depicted as in Fig. 2.5. The rate of change of the number density of $n_v, n_g$-clusters for $\rho_{v,g}$ is given by

$$\frac{d\rho_{v,g}}{dt} = J_{v-1,g}^v - J_{v.g}^v + J_{v,g-1}^g - J_{v,g}^g, \tag{2.31}$$

where

$$J_{v,g}^v = C_{v,g}^v \rho_{v,g} - E_{v+1,g}^v \rho_{v+1,g}, \tag{2.32}$$

represents the net transition of $n_v, n_g$-mers to $(n_v + 1, n_g)$-mers.

The transition from $n_{v,g}$ to $n_{v,g+1}$ clusters is given by $J_{v,g}^g$ and is equal to

$$J_{v,g}^g = C_{v,g}^g \rho_{v,g} - E_{v,g+1}^g \rho_{v,g+1}. \tag{2.33}$$
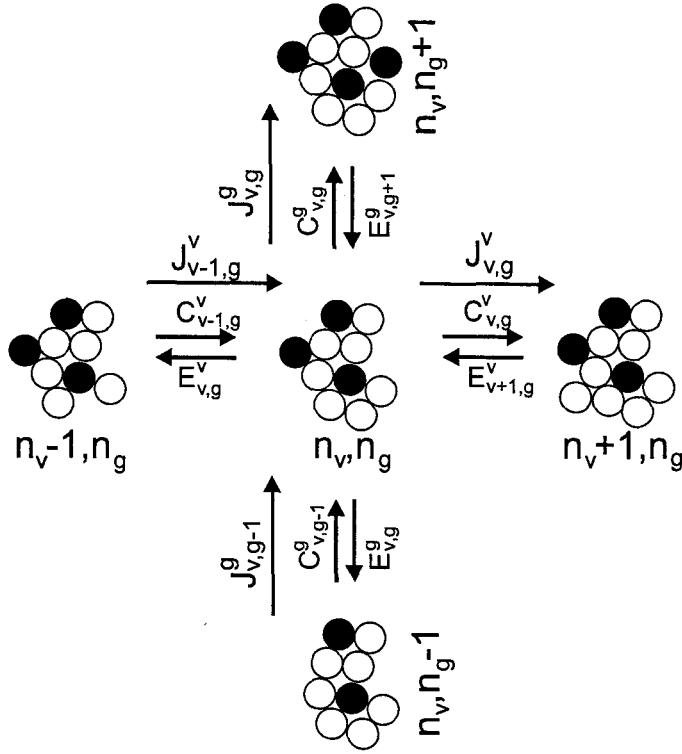
Figure 2.5: *Schematic picture of binary nucleation kinetics. $C^v_{v,g}$ and $E^v_{v,g}$ are condensation and evaporation rates for vapour molecules, $C^g_{v,g}$ and $E^g_{v,g}$ correspond to the gas molecules. Also $J^v_{v,g}$ is the net transition from $n_v, n_g$ to $n_v + 1, n_g$, whereas $J^g_{v,g}$ is a transition from $n_v, n_g$ to $n_v, n_g + 1$ clusters.*

The condensation rates $C^v_{v,g}$ and $C^g_{v,g}$ are given by

$$C^v_{v,g} = \tilde{a}_0 (n_v + n_g)^{2/3} \rho_{1,0} \left( \frac{k_B T}{2 \pi m_v} \right)^{1/2} \tag{2.34}$$

and

$$C^g_{v,g} = \tilde{a}_0 (n_v + n_g)^{2/3} \rho_{0,1} \left( \frac{k_B T}{2 \pi m_g} \right)^{1/2}. \tag{2.35}$$

The molecular surface area $\tilde{a}_0$ is equal to

$$\tilde{a}_0 = (36\pi)^{1/3} \left( \frac{n_v}{n_v + n_g} v^l_v + \frac{n_g}{n_v + n_g} v^l_g \right)^{2/3}. \tag{2.36}$$

Dividing Eq. (2.35) by Eq. (2.34) gives

$$\frac{C^g_{v,g}}{C^v_{v,g}} = \frac{\rho_{0,1} m_g^{1/2}}{\rho_{1,0} m_v^{1/2}}. \tag{2.37}$$

For a binary mixture with very small vapour fraction in the gas phase $\rho_{0,1} \gg \rho_{1,0}$. For the n-nonane and methane mixture $m_v > m_g$. This gives for the impingement rates $C_{v,g}^g \gg C_{v,g}^v$. For the case of a mixture of n-nonane and methane we can say that the nucleation rates for the vapour and gas phase are approximately of the same order, $O(J_{v,g}^g) = O(J_{v,g}^v)$. And thus $J_{v,g}^g \ll C_{v,g}^g \rho_{v,g}$ resulting in

$$C_{v,g}^g \rho_{v,g} \approx E_{v,g+1}^g \rho_{v,g+1}. \tag{2.38}$$

The equilibrium condition for $n_g$ (detailed balance condition for $n_g$) in the binary case is

$$C_{v,g}^{g\,eq} \rho_{v,g}^{eq} = E_{v+1,g}^{g\,eq} \rho_{v+1,g}^{eq}. \tag{2.39}$$

As in the unary case one can assume that the evaporation coefficient is independent of the gas content of the surroundings leading to $E_{v,g+1}^g = E_{v+1,g}^{g\,eq}$, and thus $C_{v,g}^g \approx C_{v,g}^{g\,eq}$. Dividing Eq. (2.38) by Eq. (2.39) gives

$$\frac{\rho_{v,g}}{\rho_{v,g}^{eq}} \approx \frac{\rho_{v,g+1}}{\rho_{v,g+1}^{eq}}, \tag{2.40}$$

which means that the relative deviation from equilibrium of a $v$-cluster is independent of the number of $g$-molecules in the cluster.

The net transition from clusters with $n_v$ molecules to $n_v+1$-clusters regardless of the amount of $g$-molecules present in the cluster is equal to

$$J_v = \sum_{n_g=0}^{\infty} J_{v,g}^v = \sum_{n_g=0}^{\infty} [C_{v,g}^v \rho_{v,g} - E_{v+1,g}^v \rho_{v+1,g}]. \tag{2.41}$$

The rate of change from $n_v$ to $n_v+1$-mers regardless of the number of gas-molecules present in the cluster is given by

$$\frac{d\rho_v}{dt} = \sum_{n_g=0}^{\infty} [J_{v-1,g} - J_{v,g}]. \tag{2.42}$$

The equilibrium condition for $n_v$ (detailed balance condition for $n_v$) in the binary case is

$$C_{v,g}^{v\,eq} \rho_{v,g}^{eq} = E_{v+1,g}^{v\,eq} \rho_{v+1,g}^{eq}. \tag{2.43}$$

For steady state nucleation in $n_v$:

$$\sum_{n_g=0}^{\infty} J_{v,g}^v = J_v = J. \tag{2.44}$$

For the evaporation rate the same assumption is taken as in the unary case, so $E_{v+1}^v = E_{v+1}^{v\,eq}$. This gives for $J_{v,g}^v$ using Eqs. (2.32) and (2.43):

$$\frac{J_{v,g}^v}{C_{v,g}^{v\,eq} \rho_{v,g}^{eq}} = \frac{C_{v,g}^v \rho_v}{C_{v,g}^{v\,eq} \rho_{v,g}^{eq}} - \frac{\rho_{v+1,g}}{\rho_{v+1,g}^{eq}}. \tag{2.45}$$

Summation over g-space from $n_g = 0$ to $\infty$ yields

$$J = \sum_{n_g=0}^{\infty} C_{v,g}^{v\,eq} \rho_{v,g}^{eq} \left[ \frac{C_{v,g}^{v} \rho_v}{C_{v,g}^{v\,eq} \rho_{v,g}^{eq}} - \frac{\rho_{v+1,g}}{\rho_{v+1,g}^{eq}} \right]. \tag{2.46}$$

We can say that the supersaturation $S$ for the vapour phase is equal to $S = C_{v,g}^{v}/C_{v,g}^{v\,eq}$, provided that the vapour phase mainly consists of monomers. The term in brackets can than be put in front of the summation as, according to Eq. (2.40), it doesn't depend on $n_g$, resulting in

$$\frac{J}{\sum_{n_g=0}^{\infty} C_{v,g}^{v\,eq} \rho_{v,g}^{eq}} = \frac{\rho_v}{\rho_{v,g}^{eq} S} - \frac{\rho_{v+1,g}}{\rho_{v+1,g}^{eq}}. \tag{2.47}$$

As in the unary case both sides are divided by $S^{n_v+1}$ giving

$$\frac{J}{\sum_{n_g=0}^{\infty} C_{v,g}^{v} \rho_{v,g}^{eq} S^{n_v}} = \frac{\rho_{v,g}}{\rho_{v,g}^{eq} S^{n_v}} - \frac{\rho_{v+1,g}}{\rho_{v+1,g}^{eq} S^{n_v+1}}. \tag{2.48}$$

Summing this expression left and right from $n_v = 1$ to $N_v$ gives due to cancellation of successive terms on the right hand side

$$J \sum_{n_v=1}^{N_v} \left( \frac{1}{\sum_{n_g=0}^{\infty} C_{v,g}^{v} \rho_{v,g}^{eq} S^{n_v}} \right) = 1 - \frac{\rho_{N_v+1,n_g}}{\rho_{N_v+1,n_g}^{eq} S^{n_v+1}}. \tag{2.49}$$

The last term vanishes for large enough $N_v$. Taking the limit of $N_v$ to $\infty$ gives the nucleation rate for the binary case

$$J = \left[ \sum_{n_v=1}^{\infty} \frac{1}{\sum_{n_g=0}^{\infty} C_{v,g}^{v} \rho_{v,g}^{eq} S^{n_v}} \right]^{-1}. \tag{2.50}$$

Or by replacing the summations by integrals:

$$J = \left[ \int_{=1}^{\infty} \frac{1}{\int_0^{\infty} C_{v,g}^{v} \rho_{v,g}^{eq} S^{n_v} \mathrm{d}n_g} \mathrm{d}n_v \right]^{-1}. \tag{2.51}$$

## 2.2.2   A Binary Nucleation Model

[1] The number density of $n_{v,g}$-clusters can be described by a Boltzmann-law

$$\rho_{v,g} \propto \exp\left( -\frac{\Delta G_{v,g}}{k_B T} \right) \tag{2.52}$$

---

[1] The term binary nucleation model could also refer to a system in which two components are supersaturated and can nucleate. In this case we have two components. One component is supersaturated the other is subsaturated. The subsaturated component participates in the nucleation process as it enters the clusters, and thus influences the nucleation.

where $\Delta G_{v,g}$ is the free energy of formation of a cluster consisting of $n_v$ vapour molecules and $n_g$ gas molecules. From thermodynamical considerations the free energy of formation in phase equilibrium is given by,

$$\Delta G_{v,g}^{eq} = \tilde{\theta} k_B T (n_t)^{2/3} + n_t k_B T (\hat{x}_v \ln(x_v/x_v^{eq}) + \hat{x}_g \ln(\hat{x}_g/\hat{x}_g^{eq})), \qquad (2.53)$$

where $n_t = n_v + n_g$, $\hat{x}_i$ is the molar fraction of component $i$ in the liquid phase and thus $\hat{x}_i = n_i/n_t$. The logarithmic terms are entropic mixing terms. The dimensionless surface tension $\tilde{\theta}$ is given by

$$\tilde{\theta} = \frac{\sigma \tilde{a}_0}{k_B T}, \qquad (2.54)$$

where $\tilde{a}_0$ is given by Eq. (2.36). This $\tilde{a}_0$ can be expressed in terms of $a_0$ of the unary case (Eq. (2.3))

$$\tilde{a}_0 = a_0 \left( \frac{n_v + \nu n_g}{n_v + n_g} \right)^{2/3}. \qquad (2.55)$$

Here $\nu = v_g^l/v_v^l$ is the ratio of molecular volumes of vapour and gas molecules. For $\tilde{\theta}$:

$$\tilde{\theta} = \theta_v \left( \frac{n_v + \nu n_g}{n_v + n_g} \right)^{2/3}. \qquad (2.56)$$

The equilibrium number density of $n_v, n_g$-cluster is thus equal to

$$\rho_{v,g}^{eq} = \rho_{1,0}^{eq} \exp \left( -\frac{\Delta G_{v,g}^{eq}}{k_B T} \right), \qquad (2.57)$$

where

$$\frac{\Delta G_{v,g}^{eq}}{k_B T} = \theta (n_v + \nu n_g)^{2/3} + n_v \ln \left( \frac{n_v}{(n_v + n_g) x_v^{eq}} \right) + n_g \ln \left( \frac{n_g}{(n_v + n_g) x_g^{eq}} \right). \qquad (2.58)$$

The product $\rho_{v,g}^{eq} S^{n_v}$ is equal to

$$\rho_{v,g}^{eq} S^{n_v} = \rho_{1,0}^{eq} \exp \left( n_v \ln S - \frac{\Delta G_{v,g}^{eq}}{k_B T} \right) = \rho_{1,0}^{eq} \exp \left( -\frac{\Delta G_{v,g}}{k_B T} \right) \qquad (2.59)$$

Which ultimately gives with Eq. (2.34), for the nucleation rate Eq. (2.50),

$$J = \rho_{1,0} \rho_{1,0}^{eq} a_0 \left( \frac{k_B T}{2\pi m_v} \right)^{1/2} \left[ \sum_{n_v=1}^{\infty} \frac{1}{\sum_{n_g=0}^{\infty} (n_v + \nu n_g)^{2/3} \exp(-\Delta G_{v,g}/k_B T)} \right]^{-1}. \qquad (2.60)$$

As in the unary theory a correction has to be made for consistency of the monomer energy of formation. The correction factor used in binary nucleation theory is $\exp(\theta + \ln(1/x_v^{eq}))$. This way the prefactor $\rho_{1,0}^{eq}$ in Eqs. (2.57) and (2.60) is equal to the actual monomer vapour density. This internally corrected theory is referred to as the *internally consistent binary theory* (ICBT).

# Chapter 3

# Diffusion Controlled Droplet Growth

## 3.1 Introduction

Droplet growth is the process in which stable liquid droplets gain molecules and thus become larger. Nuclei have to grow to droplets of macroscopic sizes in order to be detected. Therefore, droplet growth study, is an important part of experimental nucleation study.

The growth of droplets is determined by the transfer of mass towards a droplet and the simultaneous transfer of energy (latent heat) away from the droplet. The mechanism of this mass and energy flux depends to a large extent on the Knudsen number $Kn$, which is a length-scale parameter. It is defined as the ratio of the mean free path of the molecules to the diameter of the droplet. For very small Knudsen numbers, the transfer of molecules towards the droplet is governed by diffusion and the laws of continuum fluid dynamics can be used. For very large values of $Kn$ the transfer of heat and mass is dominated by the impingement rate of molecules onto the surface of the droplet and is described by gas kinetics. Droplet growth equations for the mentioned limiting cases are rather well known. However, droplets that start to grow after the nucleation stage will grow from the region of very large Knudsen numbers to the region of very small $Kn$ [2].

In the experimental procedure, n-nonane droplets can be detected when the droplet radius exceeds approximately $0.16 \mu m$. Nucleation experiments in this report are all performed at high carrier gas pressures ($> 10$ $bar$). At this condition the Knudsen number is small ($Kn < 0.015$), meaning that the droplet growth is diffusion controlled [2].

In the next section diffusion controlled droplet growth is treated. After this the method of Wilke and Lee for calculating diffusion coefficients is discussed.

## 3.2   Diffusion Controlled Droplet Growth
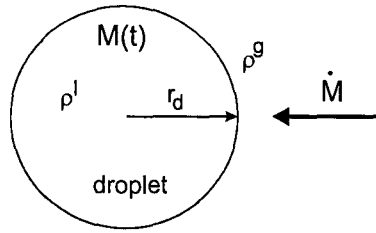


Figure 3.1: *Schematic view of a growing droplet, diffusion controlled regime.*

In Fig. 3.1 the growing droplet is shown schematically. The droplet is assumed to be spherical with radius $r_d$ and to have uniform liquid molar density $\rho^l$. The total mass of the droplet is $M$. Condensation of the gas at the droplet surface causes the droplet to grow. Condensation induces a diffusive flow of gas towards the droplet. Applying the mass balance on the time-dependent expanding surface at radius $r_d + \epsilon$, with $\epsilon \ll r_d$, gives for the mass increase of the droplet per second, $\dot{M}$:

$$\dot{M} = 4\pi r_d^2 \rho_d^g \left( \frac{\mathrm{d}r_d}{\mathrm{d}t} - u_d \right), \tag{3.1}$$

where $\rho^g$ is the molar gas density, subscript $d$ denotes that it's the density near the droplet surface. The mean molar radial velocity of the gas at the droplet surface is given by $u_d$.

In the quasi steady approach, the total induced molar flow is independent of the radius,

$$4\pi r_d^2 \rho_d^g u_d = 4\pi r^2 \rho^g u, \tag{3.2}$$

and thus

$$\dot{M} = -4\pi r^2 \rho^g u + 4\pi r_d^2 \rho_d^g \frac{\mathrm{d}r_d}{\mathrm{d}t}. \tag{3.3}$$

The increase of molar mass is by definition equal to:

$$\dot{M} = \frac{\mathrm{d}}{\mathrm{d}t} \frac{4}{3} \pi \rho^l r_d^3. \tag{3.4}$$

It is assumed that the liquid density is uniform throughout the droplet, which leads to

$$\dot{M} = 4\pi r_d^2 \rho^l \frac{\mathrm{d}r_d}{\mathrm{d}t}. \tag{3.5}$$

Combining Eqs. (3.3) and (3.5) gives

$$\rho^g u = -\frac{A_t}{4\pi r^2}, \tag{3.6}$$

where $A_t$ is equal to

$$A_t \equiv 4\pi r_d^2 (\rho^l - \rho_d^g) \frac{\mathrm{d}r_d}{\mathrm{d}t}. \tag{3.7}$$

Note that $A_t$ is a function of time only.

The same procedure can be followed for the components in the gas mixture. The total molar density of the gas phase is

$$\rho^g = \sum_j \rho_j^g, \tag{3.8}$$

where $\rho_j^g$ is the density of mixture component $j$. The velocity of each component in the mixture is equal to the sum of the bulk velocity $u$ and its diffusive velocity $v$. By definition the average of the diffusive velocity should vanish:

$$\sum_j \rho_j^g v_j = 0. \tag{3.9}$$

In a similar way as for the whole droplet, the equations for each component of the droplet can be derived. Combining

$$\dot{M}_j = -4\pi r^2 \rho_j^g (u + v_j) + 4\pi r_d^2 \rho_{d,j}^g \frac{dr_d}{dt}. \tag{3.10}$$

with

$$\dot{M}_j = 4\pi r_d^2 \rho_j^l \frac{dr_d}{dt}. \tag{3.11}$$

yields

$$A_j = -4\pi r^2 \rho_j^g (u + v_j), \tag{3.12}$$

whith

$$A_j \equiv 4\pi r_d^2 (\rho_j^l - \rho_{d,j}^g) \frac{dr_d}{dt}, \tag{3.13}$$

and

$$A_t = \sum_j A_j. \tag{3.14}$$

Combining Eqs. (3.6) and (3.12) gives

$$A_j = y_j A_t - 4\pi r^2 \rho_j^g v_j, \tag{3.15}$$

with $y_j = \rho_j^g / \rho^g$ the fraction of component $j$ in the gas phase.

When we are dealing with a diluted component, diffusive velocities can be approximated using Fick's law of diffusion [2]

$$\rho_j^g v_j = -\rho^g D_j^g \frac{d}{dr} \frac{\rho_j^g}{\rho^g}. \tag{3.16}$$

Here $D_j^g$ is the diffusion coefficient of component $j$ in the gas phase. Substituting Fick's law into Eq. (3.15) gives

$$A_j = y_j A_t + 4\pi r^2 D_j^g \frac{dr_d}{dt}. \tag{3.17}$$

As $A_j$ and $A_t$ are functions of time only, they can be integrated directly over the radius. The equation is integrated from $(r_d; y_{d,j})$ to $(r = \infty; y_{\infty,j})$. Which gives

$$(\rho^l - \rho_d^g)\frac{\mathrm{d}r_d}{\mathrm{d}t} = -\frac{\rho^g D_j^g}{r_d}\ln\left(\frac{1 - y_{\infty,j}A_t/A_j}{1 - y_{d,j}A_t/A_j}\right), \tag{3.18}$$

and

$$\frac{A_t}{A_j} = \frac{\rho^l - \rho_d^g}{\rho_j^l - \rho_{d,j}^g} \tag{3.19}$$

This expression can be simplified if $y_{\infty,j} \ll 1$, yielding

$$\frac{\mathrm{d}r_d^2}{\mathrm{d}t} = \frac{2\rho^g D_j^g}{\rho_j^l - \rho_{d,j}^g}(y_{\infty,j} - y_{d,j}). \tag{3.20}$$

## 3.3   Diffusion Coefficients

In order to use the equations derived in the previous section it is necessary to estimate diffusion coefficients for binary and ternary mixtures. To determine mixture diffusion coefficients the approach of Wilke and Lee [4] is followed. This empirically based correlation can be used to estimate diffusion coefficients in low-pressure binary gas systems. Values of the estimated diffusion coefficient with this equation generally agree with experimental values to within five to ten percent.

The theory for deriving diffusion coefficients in binary gas mixtures at low to moderate pressures has been well developed. The theory is based on solving the Boltzmann equation, which was done by Chapman and Enskog, leading to the working equation

$$D_{AB} = \frac{3}{16}\frac{(4\pi k_B T/M_{AB})^{1/2}}{n\pi\sigma_{AB}^2\Omega_D}f_D, \tag{3.21}$$

where

$$M_{AB} = 2\left[\frac{1}{M_A} + \frac{1}{M_B}\right]^{-1}. \tag{3.22}$$

Here, $M_A$ and $M_B$ are the molecular weights of component $A$ and $B$. The collision integral for diffusion $\Omega_D$ is a function of temperature and depends on the choice of intermolecular force law between colliding molecules. The characteristic length $\sigma_{AB}$ also depends on choice of the intermolecular force law. The number density of molecules in the mixture is given by $n$. Finally, $f_D$ is a correction term which is of the order of unity. If $f_D$ is chosen as unity and the ideal gas law is used to derive $n$, Eq. (3.21) can be written as

$$D_{AB} = \frac{0.00266T^{3/2}}{PM_{AB}^{1/2}\sigma_{AB}^2\Omega_D}. \tag{3.23}$$

The Wilke and Lee method rewrites this equation into

$$D_{AB} = \frac{(3.03 - (0.98/M_{AB}^{1/2})) \cdot 10^{-3}T^{3/2}}{PM_{AB}^{1/2}\sigma_{AB}^2\Omega_D}.$$

(3.24)

The scale parameter is given by

$$\sigma_{AB} = \frac{\sigma_A + \sigma_B}{2},$$

(3.25)

where for each component

$$\sigma = 1.18V_b^{1/3}$$

(3.26)

in which $V_b$ is the liquid molar volume, $cm^3/mol$, found from experimental data. The collision integral $\Omega_D$ is calculated with

$$\Omega_D = \frac{1.06036}{(T^*)^{0.15610}} + \frac{0.19300}{\exp(0.47635T^*)} + \frac{1.03587}{\exp(1.52996T^*)} + \frac{1.76474}{\exp(3.89411T^*)},$$

(3.27)

where $T^* = k_B T/\epsilon_{AB}$.

$$\epsilon_{AB} = (\epsilon_A \epsilon_B)^{1/2},$$

(3.28)

and for each component

$$\frac{\epsilon}{k_B} = 1.15T_b,$$

(3.29)

with $T_b$ as the normal boiling point.

For calculating diffusion coefficients in multicomponent gas mixtures, Blanc's law can be used:

$$D_{i,m} = \left( \sum_{j=1 \neq i}^{n} \frac{x_j}{D_{ij}} \right)^{-1}.$$

(3.30)

where $x_j$ is the molar gas fraction of component $j$. Blanc's law can be applied to ternary cases in which $i$ is a dilute component [4]. By means of Blanc's law we calculated diffusion coefficients of the vapour component for the mixture studied in this report.

# Chapter 4

# Wave Tube Experiments

## 4.1 The Nucleation Pulse Method

In order to measure nucleation and droplet growth rates, use is made of an expansion wave tube. The expansion wave tube experiment is based on the so-called nucleation pulse method, one of the most popular and successful means to determine quantitative nucleation rates. The pulse method is based on the separation in time of the nucleation and growth stages of the droplet formation process. This separation is achieved by subjecting the vapour to a proper saturation time history.

First the saturation is brought to a level that induces a significant nucleation rate. This state is maintained for a short time interval $\Delta t$, the so-called nucleation pulse. After the pulse the supersaturation is reduced, thus quenching the nucleation process. The saturation ratio is still being kept larger than unity, allowing for the nucleated clusters to grow to macroscopic sizes. This way, a monodispersed cloud of droplets is formed, which greatly facilitates the characterization in terms of radius and number density $n_d$. Division of the number density and the time duration of the nucleation pulse yields the nucleation rate, i.e. the number of droplets formed per unit time and volume

$$J = \frac{n_d}{\Delta t}. \tag{4.1}$$

The required pulse-like saturation profile is always realized by gas dynamic principles. By creating a fast (isentropic) expansion wave in a vapour-gas mixture, the temperature decreases rapidly with pressure. Due to the non-linear dependence of the saturated vapour pressure $p^s$ on temperature, the saturation ratio can be brought from below unity to very large values. The specific pulse-like time dependency of the saturation ratio is now achieved by modulating the initial expansion wave by a small recompression, see Fig. 4.1 [1].

One of the gas dynamic principles mentioned above is based on the use of a shock tube to generate the pulse. The saturation profile is created in the high pressure section of the
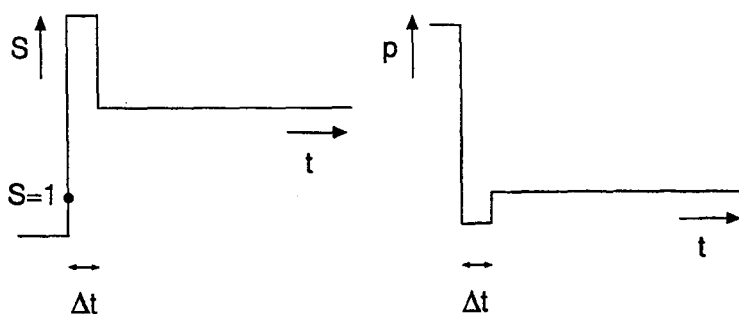
Figure 4.1: *Principle of the nucleation pulse method: schematic saturation profile and the associated pressure history required to produce it [3].*

shock tube. The pressure drop is caused by the expansion wave travelling backwards into the high pressure section. The shock wave plays a crucial role in the formation of the pulse. It reflects at a local widening in the low pressure section as another small expansion, followed by a weak recompression at the end of the widening. These reflected waves travel back into the high pressure section, creating the desired pulse-shaped expansion at the high pressure section end wall. After the pulse the pressure remains essentially constant over a longer period of time (except for some small disturbances, which are mainly due to reflections of the initial expansion wave at the local widening). The pressure plateau is finally ended by the return of the reflected shock wave from the low pressure section end wall. An $x - t$-diagram of the pressure waves in the expansion wave tube is shown in Fig. 4.2, together with the resulting pressure and temperature history at the observation point in the high pressure section [1].

## 4.2   Mixture Preparation

The nucleation rate is extremely dependent on the supersaturation. A small inaccuracy in the initial composition of the vapour/gas mixture results in large errors in the nucleation rates. Therefore, the controlled mixture preparation is of crucial importance for obtaining good experimental results.

Mixtures are prepared using a sophisticated system of tubes, valves and saturators through which the mixture flows, controlled by several mass flow controllers. The initial carrier gas is split into several branches, each one controlled by a mass flow controller. Each branch can be saturated with either n-nonane or water, at constant temperature and pressure, in the saturators, or keep its original composition. In the saturators the carrier gas is saturated either with water or n-nonane. The saturators consist of two vessels which are completely
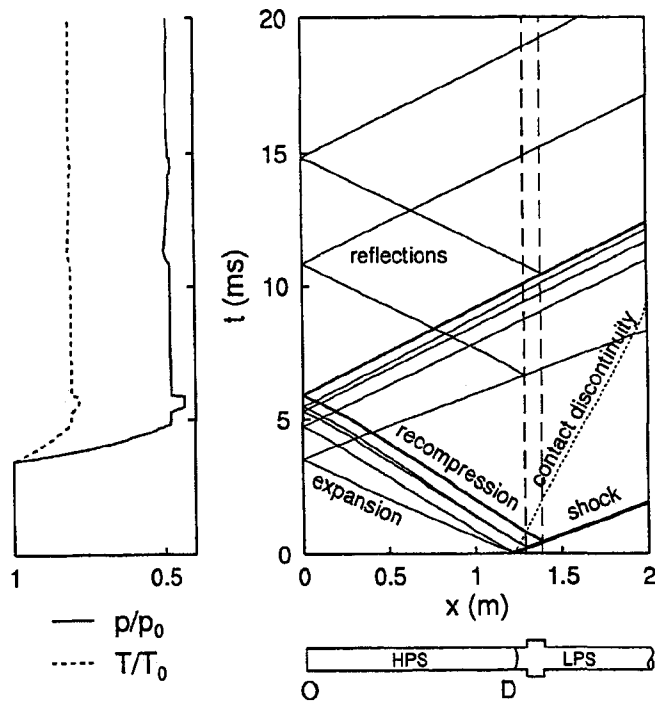
Figure 4.2: $x - t$ diagram of wave propagation in the pulse expansion wave tube, with schematic tube configuration and resulting pressure and temperature at the observation point O. The dashed lines indicate the position of the local widening; D denotes the diaphragm position [1].

filled with three layers of glass beads. The vessels are approximately half filled with either n-nonane or water. The vessels are submerged in a temperature-controlled bath. Saturation of the carrier gas is accomplished by bubbling the gas through the liquid in the vessels. This way the carrier gas gets saturated with the vapour until the equilibrium fraction of vapour is reached at the temperature and pressure in the saturators.

After passing the saturators, the two flows join and mix. Subsequently the mixture is carefully guided towards the high pressure section of the shocktube, the gas is preheated in order to avoid premature condensation.

A schematic view of the mixture preparation of the ternary mixture methane-propane-n-nonane is presented in Fig. 4.3. The initial binary mixture consists of $Y_{C1}$ methane and $Y_{C3}$ propane gas fraction. This flow is split and one part flows through the saturator and is saturated with n-nonane at the conditions in the saturator. The composition after passing the saturator is equal to $(y_{C1}^{eq}(T_{sat}, p_{sat}, Y_{C1}/Y_{C3}),\ y_{C3}^{eq}(T_{sat}, p_{sat}, Y_{C1}/Y_{C3}),$ $y_{C9}^{eq}(T_{sat}, p_{sat}, Y_{C1}/Y_{C3}))$. The equilibrium fractions have to be calculated using $T_{sat}$, $p_{sat}$
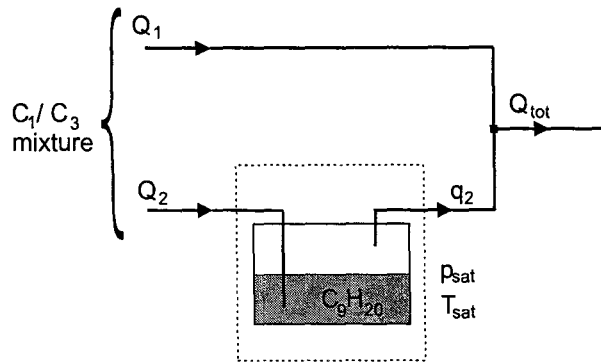
Figure 4.3: *Schematic view of the mixture preparation system for the ternary mixture of methane-propane-n-nonane.*

and the constant methane/propane fraction

$$\frac{Y_{C1}}{Y_{C3}} = \frac{y_{C1}^{eq}}{y_{C3}^{eq}}. \tag{4.2}$$

The total molecular flow is equal to

$$Q_{tot} = Q_1 + q_2. \tag{4.3}$$

For $q_2$ the following can be easily derived

$$q_2 = \frac{Q_2}{1 - \frac{y_{C9}^{eq}}{1-Y_{C1}}}. \tag{4.4}$$

The amount of nonane entering the mixture has to be calculated using an appropriate equation of state. This introduces a systematic error in the experiment depending on the choice of equation of state. The vapour fraction is essential in determining the supersaturation at nucleation conditions. Moreover, for determining the supersaturation a second equilibrium calculation has to be made to determine the equilibrium nonane vapour fraction at nucleation conditions, and thus introducing another systematic error due to the accuracy of the equation of state used for this calculation. When interpreting experimental results one has to be aware of these systematic errors as they can have a big influence on nucleation results.

## 4.3  Optical Droplet Detection

For the experimental determination of droplet size and number density, the optical setup, which is schematically shown in Fig. 4.4 is used. The cloud of droplets that are formed

during the nucleation pulse is illuminated by a solid state laser (wavelength $532nm$). The beam passes the tube through two conical windows, which are placed a bit below the tube axis to prevent interference of internal reflections.

During the growth stage, the droplets scatter part of the incident light in all directions,
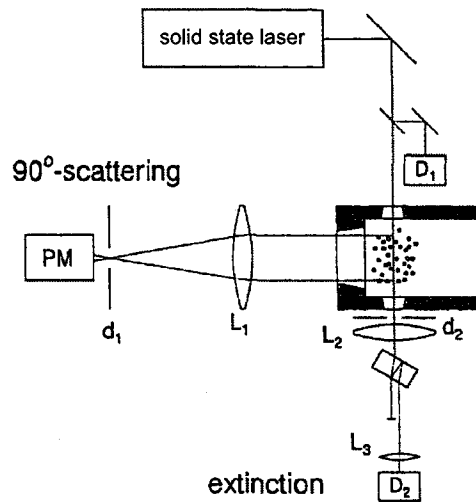


Figure 4.4: *Optical setup used for measurement of droplet size and number density, situated at the end wall of the expansion wave tube [1].*

with a characteristic pattern that is strongly dependent on the scattering angle $\theta$. The light scattered under an angle of 90° is recorded by a photomultiplier. The light which isn't scattered by the droplets is focussed on a photodiode on the other side of the tube. The transmitted light signal is normalized by the signal of a reference beam, to account for intensity fluctuations of the laser [1].

## 4.3.1   Constant Angle Mie Scattering

In the experiment the light is vertically polarized and scattered by the droplets through the end wall of the high pressure section. The scattered light is focussed on the photomultiplier. Constant Angle Mie Scattering (CAMS) is used in order to interpret the signal. CAMS is based on Mie theory, describing the scattering of plane electro-magnetic waves by dielectric particles of arbitrary size. For particle sizes of the order of the incident wavelength, the scattered irradiance shows a typical pattern of extrema. This pattern can be calculated as function of the dimensionless parameter $\alpha = 2\pi r_d/\lambda$, for a fixed scattering angle and index of refraction $m$ of the liquid droplets. In a nucleation pulse experiment, where a nearly monodispersed droplet population is evolving in time, these extrema show up consecutively.

By mapping the experimental extrema to the theoretical ones, each droplet radius $r_d$ can be assigned to a point in time, making it possible to construct an experimental droplet growth curve.

This procedure is illustrated in Fig. 4.5, for an experiment in n-nonane-helium. In high
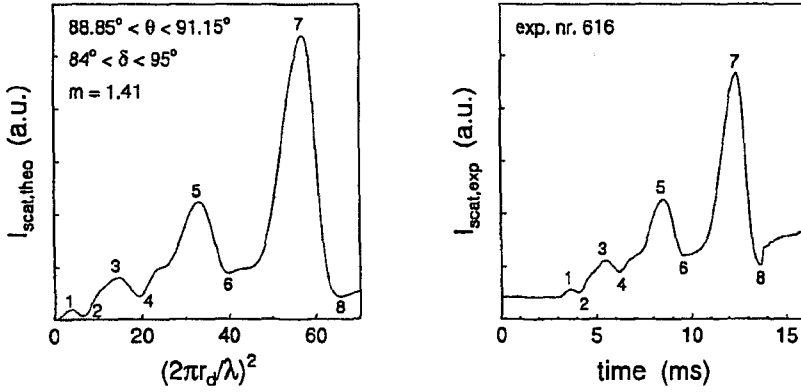


Figure 4.5: *Theoretical and experimental scattering patterns for n-nonane droplets. From the mutual correspondence of extrema the time-resolved radius $r_d(t)$ is obtained [1].*

pressure experiments, CAMS can also be used, however the number of extrema that can be observed in the finite observation time is smaller compared to low pressure experiments. This is because at high pressures diffusion processes proceed at a lower rate [1].

## 4.3.2 Light Extinction

The number density of droplets is determined using light extinction measurements, this method is based on Lambert-Beer's law

$$I = I_0 \exp(-\beta l), \tag{4.5}$$

where $I$ is the transmitted light density, $l$ is the optical path length through the droplet cloud (equal to 36mm in the experiments). The extinction coefficient $\beta$ is given by

$$\beta = n_d \pi r_d^2 Q_{ext}(\alpha, m). \tag{4.6}$$

The extinction efficiency $Q_{ext}$ depends on the size parameter $\alpha = 2\pi r_d/\lambda$ and the index of refraction $m$, which can be calculated from Mie theory. Together with the attenuation $I/I_0(t)$ the number density $n_d$ can be found, which should be approximately constant, in the ideal case, it would only vary due to small pressure fluctuations during the growth period. But in practice there is some more scatter due to changes in reflection index and

dynamic forces acting on the tube during wave propagation, but these are minimized by careful alignment of the optical setup [1].

# Chapter 5

# Phase Equilibrium Models

## 5.1 Supersaturation

As can be seen in Fig. 6.1, nucleation rates are strongly dependent on the supersaturation. It is therefore crucial to accurately know the supersaturation. The degree of supersaturation is characterized by the chemical potential difference between the actually existing non-equilibrium state and the corresponding phase equilibrium. For the case of a pure vapour, the supersaturation $S$ is defined as

$$S = \exp\left[\frac{\mu^v(p, T, y_v) - \mu^v(p, T, y_v^{eq})}{k_B T}\right],$$ (5.1)

where $y_v$ is the actual vapour fraction present in the mixture, which can be different from its equilibrium value $y_v^{eq}$. This equation can be rewritten, using some thermodynamics, into

$$S = \frac{\phi_v y_v p}{\phi_v^{eq} y_v^{eq} p}.$$ (5.2)

In this expression $\phi_v$ and $\phi_v^{eq}$ are the fugacity coefficients, that account for the intermolecular forces that a vapour molecule experiences from its surroundings. Since vapour fractions in both the supersaturated and equilibrium states are very small, $\phi_v$ and $\phi_v^{eq}$ are equal to one another to a high degree of approximation. Therefore Eq. (5.2) can be approximated as [1]

$$S \simeq \frac{y_v}{y_v^{eq}},$$ (5.3)

thus the supersaturation is simply a measure for the overpopulation of the vapour phase.

## 5.2 RKS Equation of State

The actual vapour fraction $y_v$ is determined by the nucleation experiment. Equilibrium vapour fractions have to be calculated using a proper equation of state (EOS) or equilibrium

experiments. For the cases investigated in this report, experimental data is not present. For n-nonane-methane mixtures it was concluded on the basis of experimental data [5], that the Redlich-Kwong-Soave (RKS) equation yielded the smallest overall error in composition [1].

The RKS EOS is given by:

$$p = \frac{RT}{V - b} - \frac{a(T)}{V(V + b)},$$                                     (5.4)

where $a(T)$ depends on temperature according to

$$a(T) = \frac{0.42748R^2T_c^2}{p_c}\left[1 + f(\omega)\left(1 - \sqrt{\frac{T}{T_c}}\right)\right]^2$$              (5.5)

with

$$f(\omega) = 0.48 + 1.574\omega - 0.176\omega^2.$$                                  (5.6)

In these equations, $R$ is the universal gas constant, $V$ is the molar volume, $\omega$ is Pitzer's acentric factor and the subscript $c$ refers to the critical point. The constant $b$ is given by

$$b = \frac{0.08664RT_c}{p_c}.$$                                                    (5.7)

For a mixture, $a$ and $b$ are evaluated from the pure component values using the mixing rules

$$a_m = \sum_i \sum_j y_i y_j (a_i a_j)^{1/2}(1 - k_{ij})$$                          (5.8)

$$b_m = \sum_i y_i b_i,$$                                                           (5.9)

which are valid for simple mixtures of nonpolar components. The binary interaction parameters $k_{ij}$ can be evaluated by fitting $k_{ij}$ to binary vapor-liquid equilibria from an equation of state. For simple systems, $k_{ij}$ is often nearly independent of temperature [6].


## 5.3   Phase Equilibria 2000 Program

The program PE (Phase Equilibria) has been developed at the Technical University of Hamburg-Harburg, starting in 1985. PE was built in order to obtain an efficient tool to correlate phase equilibria, especially those at high pressure that are related to gas-extraction processes. PE offers more than 40 different equations of state (EOS) with up to seven different mixing rules for correlating and predicting phase equilibria. PE offers subroutines to determine optimum binary interaction parameters for all EOS in order to reproduce the phase behavior of binary and ternary systems with a given set of EOS and mixing rule [7]. The PE program is used for calculating phase equilibria in binary and ternary mixtures.

Binary interaction parameters were also calculated by this program using experimental data. With the phase equilibria data calculated by the program, fitting curves were made, resulting in phase equilibrium calculation models.

## 5.3.1  N-Nonane-Methane System

The first system which is looked at is the binary n-nonane-methane mixture. Nucleation of this mixture was examined in chapter 6. This binary mixture forms also the basis of the ternary mixtures examined in the next sections. For calculation of the binary interaction parameter $k_{ij}$ for this mixture, experimental data of Shipman and Kohn [5]. This resulted in the following equation for $k_{ij}$ for n-nonane-methane

$$k_{C_1,C_9} = k_{C_9,C_1} = 4.558 \cdot 10^{-2} + 2.19966 \cdot 10^{-5}T. \tag{5.10}$$

Using the PE-program, phase equilibria can be calculated. With the use of the Gibb's phase rule, the number of degrees of freedom in the system can be calculated:

$$F = m + 2 - \pi, \tag{5.11}$$

where $m$ is the number of components and $\pi$ the number of phases. We are looking at a binary mixture in liquid-gas phase equilibrium, resulting in two degrees of freedom [6]. For convenience the degrees of freedom are chosen to be the temperature $T$ and the pressure $p$. The range of temperatures is for experimental purposes chosen between 230 and 320K. Pressures range from 5 to 40 bar. The PE program calculates phase equilibrium compositions in this range. Making fits through these equilibrium points leads to equations for calculating phase equilibrium for this mixture using the RKS equation of state.

An equation for the phase equilibrium vapor fraction of n-nonane is necessary for the determination of the supersaturation in nucleation experiments. The fit for the equilibrium n-nonane molar fraction in the gas phase for the given temperature and pressure range according to RKS is given by:

$$y_{C_9}^{eq} = y_0^{C_9}(p) \exp(y_1^{C_9}(p) + y_2^{C_9}(p)T + y_3^{C_9}(p)T^2), \tag{5.12}$$

where $p$ and $T$ are dimensionless pressure and temperature. Equations for $y_{0..3}^{C_9}(p)$ can be found in appendix B together with equations for $x_{C_9}^{eq}$, $x_{C_1}^{eq}$ and $y_{C_1}^{eq}$.

The accuracy of this model can be compared to experimental data [5]. Table 5.1 compares experimental values for the molar fraction of methane in the liquid phase $x_{C_1}$ with values calculated using the model in appendix B. In this table the error $\delta$ is given by

$$\delta = \frac{x_{C_1}^{exp} - x_{C_1}^{fit}}{x_{C_1}^{exp}}. \tag{5.13}$$

| $T(K)$ | $P(bar)$ | $x_{C_1}^{exp}$ | $x_{C_1}^{fit}$ | $\delta(\%)$ |
|--------|----------|------------------|------------------|--------------|
| 298.15 | 10.1325  | 0.0509           | 0.04703          | 7.61         |
| 298.15 | 20.2650  | 0.0986           | 0.09084          | 7.87         |
| 298.15 | 30.3975  | 0.1426           | 0.13170          | 7.65         |
| 298.15 | 40.5300  | 0.1832           | 0.17102          | 6.65         |
| 273.15 | 10.1325  | 0.0540           | 0.05514          | −2.12        |
| 273.15 | 20.2650  | 0.1069           | 0.10569          | 1.14         |
| 273.15 | 30.3975  | 0.1563           | 0.15203          | 2.73         |
| 273.15 | 40.5300  | 0.2023           | 0.19642          | 2.91         |
| 248.15 | 10.1325  | 0.0678           | 0.06871          | −1.35        |
| 248.15 | 20.2650  | 0.1288           | 0.13037          | −1.22        |
| 248.15 | 30.3975  | 0.1856           | 0.18557          | 0.02         |
| 248.15 | 40.5300  | 0.2381           | 0.23793          | 0.07         |
| 223.15 | 10.1325  | 0.0989           | 0.08910*         | 9.91         |
| 223.15 | 20.2650  | 0.1737           | 0.16952*         | 2.41         |
| 223.15 | 30.3975  | 0.2418           | 0.24173*         | 0.03         |
| 223.15 | 40.5300  | 0.3033           | 0.30607*         | −0.91        |

Table 5.1: *Experimental phase equilibrium data for the n-nonane-methane system by Shipman and Kohn [5] compared to calculated equilibrium data using the fit in appendix B for the binary n-nonane-methane system. Values with * are outside the modelling range.*

As can be seen in this table, errors are within 10%. At low temperatures, the error is no more than 5%. In the chapter on numerical calculations, the temperature of interest was $240K$, equilibrium calculations at this temperature seem to be quite accurate compared to the experimental data.

## 5.3.2  N-Nonane-Methane-Carbon Dioxide System

Because of interest in ternary mixture phase equilibria, the mixture n-nonane, methane and carbon dioxide was investigated. Following Gibb's phase rule Eq. (5.11), this system has three degrees of freedom. These are pressure, temperature and fraction of carbon dioxide in the gas phase, as these three parameters can be controlled during the experiments.

The range of temperatures is for experimental purposes chosen between 230 and 320K. Pressures range from 5 to 40 bar. The fraction of carbon dioxide in the gas phase ranges from 0 to 3%.

To calculate phase equilibria for a ternary mixture using RKS requires three binary interaction parameters. The n-nonane-methane interaction parameter is given by Eq. (5.10). The

interaction parameter for n-nonane and carbon dioxide was calculated using experimental data from Jennings and Schucker [8] which gives using the PE program

$$k_{C_9,CO_2} = k_{CO_2,C_9} = 0.10363. \tag{5.14}$$

The binary interaction parameter for methane and carbon dioxide was derived using experimental data from Kidnay and Wei [9] resulting in the following interaction parameter

$$k_{C_1,CO_2} = k_{CO_2,C_1} = 0.09718. \tag{5.15}$$

From PE data it appears that $y_{C_9}^{eq}$ is only slightly dependent on $y_{CO_2}^{eq}$. In the fit this dependence is neglected this results for $y_{C_9}^{eq}$ into

$$y_{C_9}^{eq} = y_0^{C_9}(p) \exp(y_1^{C_9}(p) + y_2^{C_9}(p)T + y_3^{C_9}(p)T^2), \tag{5.16}$$

where $p$ and $T$ are dimensionless pressure and temperature. Equations for $y_{0..3}^{C_9}(p)$ can be found in appendix B together with equations for $x_{C_9}^{eq}$, $x_{C_1}^{eq}$, $x_{CO_2}^{eq}$ and $y_{C_1}^{eq}$.
If in these equations, $y_{CO_2}^{eq}$ is taken equal to 0, the equations simplify to the n-nonane-methane mixture equations. There is no experimental data for this ternary mixture within the chosen range, except for the limiting binary n-nonane-methane system treated in the previous section. The accuracy of the fit in comparison with the calculated equilibrium points by the PE program is illustrated in Fig. 5.1. Errors are all within 1% of the PE data. For the rest of the components in the mixture, errors are within 5% of the PE data.

### 5.3.3  N-Nonane-Methane-Propane System

The final mixture under consideration is the ternary mixture of n-nonane, methane and propane. This mixture is treated in the experimental section of this report. As in the previous ternary mixture there are three degrees of freedom. Temperature, pressure and the propane molar fraction in the gas phase are chosen for this purpose.
The range of temperatures is for experimental purposes chosen between 225 and 245K. Pressures range from 6 to 14 bar. The fraction of propane in the gas phase ranges from 0 to 2%.
To calculate phase equilibria for a ternary mixture using RKS requires three binary interaction parameters. The n-nonane-methane interaction parameter is given by Eq. (5.10). The interaction parameter for n-nonane and propane was calculated using experimental data from Jennings and Schucker [8] which gives using the PE program

$$k_{C_9,C_3} = k_{C_3,C_9} = -0.01967. \tag{5.17}$$

The binary interaction parameter for methane and propane was derived using experimental data from Webster and Kidnay [10] resulting in the following interaction parameter

$$k_{C_1,C_3} = k_{C_3,C_1} = 0.6396 - 0.00509T + 1.03034 \cdot 10^{-5}T^2. \tag{5.18}$$

Figure 5.1: *Comparison of PE data points and fit for $y_{C_9}^{eq}$ as function of $y_{CO_2}^{eq}$ based on these data points for the ternary system of n-nonane, methane and carbon dioxide.*

From PE data it appears that for $y_{C_9}^{eq}$ in this system the dependence on $y_{C_3}^{eq}$ is not negligible. The fit for the n-nonane fraction for this system is given by

$$
\begin{aligned}
y_{C_9}^{eq} = {} & \exp(y_0^{C_9}(p) + y_1^{C_9}(p)T + y_2^{C_9}(p)T^2) + \\
& + y_{C_3}^{eq}\left[\exp(y_3^{C_9}(p) + y_4^{C_9}(p)T + y_5^{C_9}(p)T^2)\right],
\end{aligned}
\tag{5.19}
$$

where $p$ and $T$ are dimensionless pressure and temperature. Equations for $y_{0..5}^{C_9}(p)$ can be found in appendix B together with equations for $x_{C_9}^{eq}$, $x_{C_1}^{eq}$, $x_{C_3}^{eq}$ and $y_{C_1}^{eq}$.

The equations of this mixture do not reduce to the binary n-nonane-methane mixture treated before, when setting $y_{C_3}^{eq}$ to zero, as the modelling range is different. There is no experimental data for this ternary mixture within the chosen range. The only data present is the Shipman data [5] for the binary case, but all these experimental points are outside the modelling range. However the data is compared with the model in appendix B, as can be seen in table 5.2. In this table the error $\delta$ is given by

$$
\delta = \frac{x_{C_1}^{exp} - x_{C_1}^{fit}}{x_{C_1}^{exp}}.
\tag{5.20}
$$

All values in this table are outside the modelling range, so it is difficult to make conclusions. For pressures inside the modelling range, the errors seem reasonable.

The accuracy of the fit in comparison with the calculated equilibrium points by the PE

| $T(K)$ | $P(bar)$ | $x_{C_1}^{exp}$ | $x_{C_1}^{fit}$ | $\delta(\%)$ |
|--------|----------|-----------------|-----------------|--------------|
| 273.15 | 10.1325 | 0.0540 | 0.05429* | −0.54 |
| 273.15 | 20.2650 | 0.1069 | 0.11824* | −10.61 |
| 248.15 | 10.1325 | 0.0678 | 0.06613* | 2.46 |
| 248.15 | 20.2650 | 0.1288 | 0.15109* | −17.31 |
| 223.15 | 10.1325 | 0.0989 | 0.08789* | 11.14 |
| 223.15 | 20.2650 | 0.1737 | 0.21043* | −21.14 |

Table 5.2: *Experimental phase equilibrium data for the n-nonane-methane system by Shipman and Kohn [5] compared to calculated equilibrium data using the fit in appendix B for the ternary system n-nonane-methane-propane. Values with * are outside the modelling range.*

program is illustrated in Fig. 5.2. Errors are all within 1% of the PE data. For the rest of the components in the mixture, errors are within 5% of the PE data.
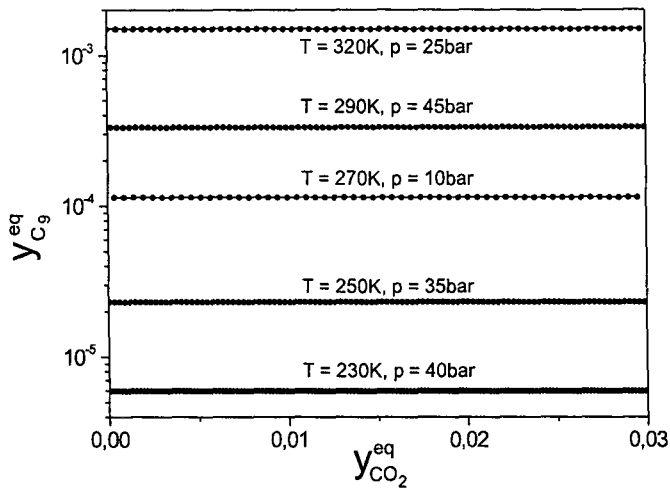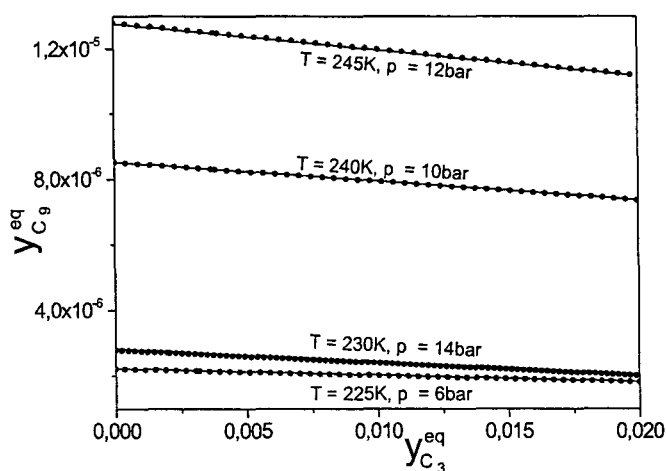


Figure 5.2: *Comparison of PE data points and fit for $y_{C_9}^{eq}$ as function of $y_{C_3}^{eq}$ based on these data points for the ternary system of n-nonane, methane and propane.*

# Chapter 6

# Numerical Nucleation Calculations

## 6.1 Nucleation Behaviour of n-Nonane-Methane Mixtures

Starting point in this chapter are the experimental results from nucleation experiments of supersaturated n-nonane ($C_9H_{20}$) in a carrier gas of methane ($CH_4$). Experiments were performed at Eindhoven University of Technology by several experimenters. The experiments were performed at a constant nucleation temperature of 240K, at varying pressures. Results of these experiments are displayed in Fig. 6.1.

As can be seen in this figure, there is a clear pressure dependency in nucleation behaviour for these series of experiments. First an increase of nucleation rate with increasing pressure can be observed. Secondly, if a fit is made through experimental data at the same pressure, a decrease in slope with increasing pressure is found.

In the remainder of this chapter, nucleation theory will be examined to see whether it is able to predict this pressure trend. In the following sections, binary nucleation theory will be examined, and in several steps extended in order to study the effect on nucleation behaviour. In the first section, examination of the theory will start with ideal nucleation behaviour, and will be extended into several steps to Langmuir surface tension correction. This in order to find a possible explanation of the pressure dependence of the nucleation rate of n-nonane in a carrier gas of methane.

From the theoretical study a possible explanation of the pressure trend might also be formulated.
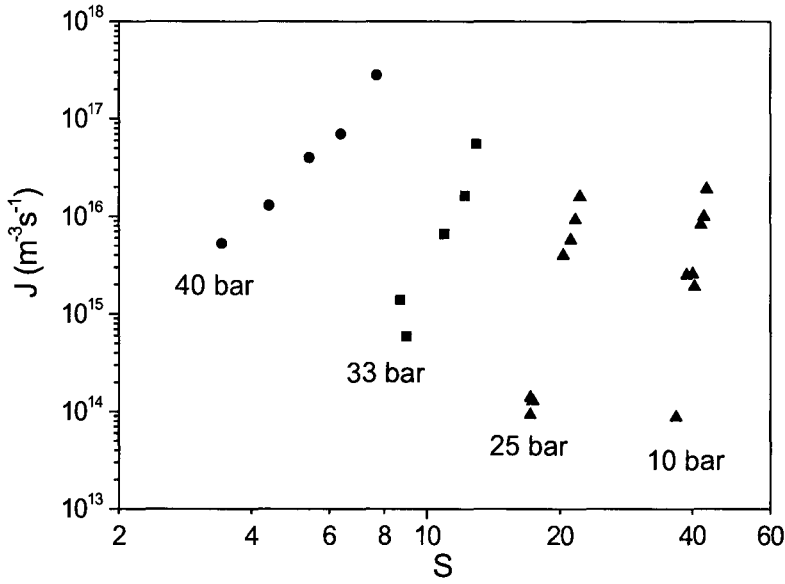
Figure 6.1: *Experimental temperature-corrected nucleation rates for a n-nonane-methane mixture at 240K, 40 bar experiments by Peeters (circles), 33 bar experiments by Labetski (squares), 25 bar and 10 bar experiments by Luijten (triangles).*

### 6.1.1   Ideal Binary Nucleation Theory

As a first approach the unary nucleation theory can be used to calculate nucleation rates [1]:

$$J = \rho_1 \rho_1^{eq} v_v^l \left( \frac{2\sigma}{\pi m_v} \right)^{1/2} \exp \left[ \theta - \frac{4}{27} \frac{\theta^3}{(\ln S)^2} \right]. \tag{6.1}$$

The binary nucleation theory can also be used, if the logarithmic mixing terms are neglected we get:

$$J = \rho_{1,0} \rho_{1,0}^{eq} a_0 \left( \frac{k_B T}{2\pi m_v} \right)^{1/2} \left[ \sum_{n_v=1}^{\infty} \frac{1}{\sum_{n_g=0}^{\infty} (n_v + \nu n_g)^{2/3} \exp(-\Delta G_{v,g}/k_B T)} \right]^{-1}, \tag{6.2}$$

with

$$\frac{\Delta G_{v,g}}{k_B T} = -\theta + \theta (n_v + \nu n_g)^{2/3} + n_v \ln S. \tag{6.3}$$

The additional $\theta$ in the right hand side of Eq. (6.3) is to guarantee consistency for the monomer density.

In order to apply the model to a specific case, some of the constants need to be specified.

In the first case, ideal gas behaviour is assumed. This gives for the equilibrium n-nonane monomer density

$$\rho_{1,0}^{eq} = \rho_1^{eq} = \frac{p^s}{k_B T},$$ (6.4)

where $p^s$ is the saturation pressure of n-nonane and is given in appendix A together with other physical properties for n-nonane. The non-equilibrium density is equal to the equilibrium density times the supersaturation:

$$\rho_{1,0} = \rho_1 = \frac{S p^s}{k_B T}.$$ (6.5)

With these equations and the data in appendix A, theoretical predictions can be made. Without the mixing terms present in the equation, the nucleation rate is independent of pressure. The results for unary and binary theory under the given assumptions can be found in Fig. 6.2 for several nucleation temperatures. For the surface tension, the pure nonane surface tension is used at corresponding temperatures as given in appendix A.

As already mentioned before, there is no pressure dependence in the case considered. This
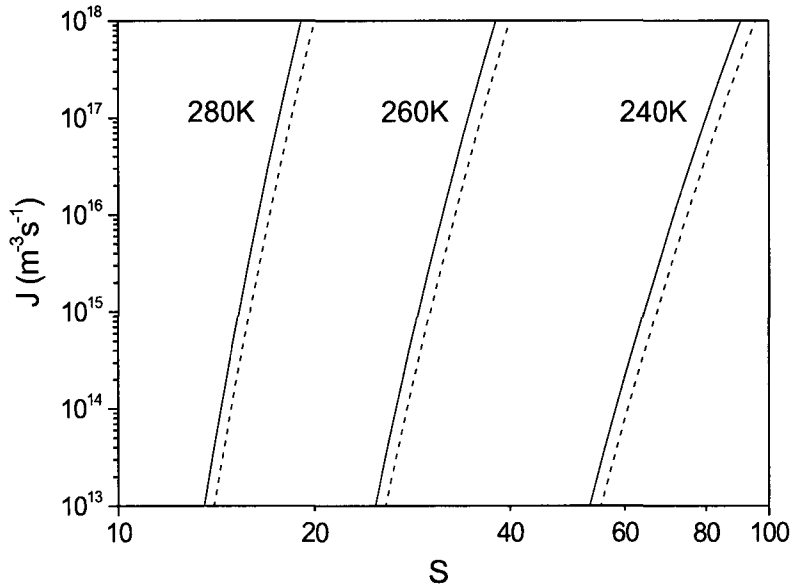


Figure 6.2: *Theoretical calculations for nucleation of n-nonane in methane at several temperatures using ideal unary (dashed line) and binary theory (solid line), neglecting entropic mixing terms. For the surface tension, the pure nonane surface tension is used at corresponding temperatures.*

case assumes ideal gases, neglecting entropic mixing terms. For the surface tension, the pure

nonane surface tension is used at corresponding temperatures. There is a clear temperature dependence mainly caused by the dependance of surface tension on temperature. Higher nucleation temperatures give rise to higher nucleation rates for the same supersaturation. Classical unary theory predicts a slightly lower nucleation rate compared to binary theory. Both theories give a similar temperature trend. In comparison with experimental results, it can be concluded that for this case the theoretical nucleation rates are many orders of magnitude below experimental values for 240K.

## 6.1.2   Ideal Nucleation Theory with Mixing Terms

In the previous assumption, pure n-nonane clusters were considered. In the case of n-nonane in a carrier gas of methane, dissolving of methane molecules into the cluster can be expected. A first approach to account for this effect is by implementing the entropic mixing terms into the binary theory. Methane molecules enter the cluster for entropic reasons only. This extends Eq. (6.3) into [11]

$$
\begin{aligned}
\frac{\Delta G_{v,g}}{k_B T} = &-\theta - \ln\left(\frac{1}{x_v^{eq}}\right) + \theta(n_v + \nu n_g)^{2/3} + n_v \ln S \\
&+ n_v \ln\left(\frac{n_v}{(n_v + n_g)x_v^{eq}}\right) + n_g \ln\left(\frac{n_g}{(n_v + n_g)x_g^{eq}}\right).
\end{aligned}
\tag{6.6}
$$

Notice the additional logarithmic correction term for consistency. By including these mixing terms, a pressure dependency is introduced into the theory: the equilibrium molar fraction of n-nonane in the liquid phase $x_v^{eq}$ has a pressure dependency as well as a temperature dependency. This value can be calculated from equilibrium models which are also presented in this report. These models assume a flat surface equilibrium between liquid and gas phase. They are based on the RKS equation of state and will be presented later. For the surface tension, the pure nonane surface tension is used at corresponding conditions. The numerical results for this theory for a nucleation temperature of 240K at three pressures are shown in Fig. 6.3.

This case assumed ideal gases. Entropic mixing terms were introduced. For the surface tension, the pure nonane surface tension is used at corresponding conditions. From this figure it becomes clear that the effect of the mixing term does not have a large effect on nucleation rates. Moreover the pressure dependence is opposite to the effect observed in the experimental results (Fig. 6.1). By introducing the logarithmic term an increase of pressure leads to lower nucleation rates.
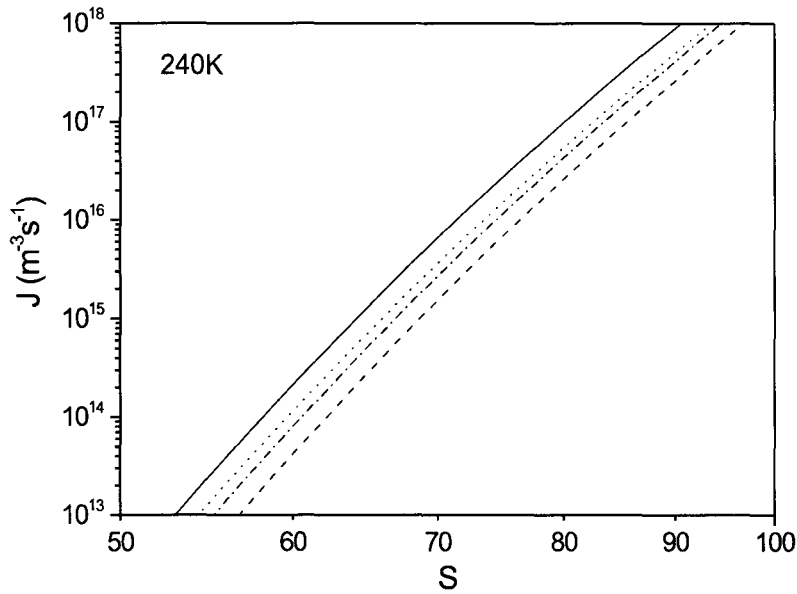
Figure 6.3: *Theoretical calculations for nucleation of n-nonane in methane at 240K at pressures of 10 bar, $x_v^{eq} = 0.93$ (dotted line), 25 bar, $x_v^{eq} = 0.83$ (dash-dotted line) and 40 bar, $x_v^{eq} = 0.75$ (dashed line) using binary theory with mixing terms and nucleation at 240K without mixing terms (dashed line).For the surface tension, the pure nonane surface tension is used at corresponding conditions.*

### 6.1.3 Non-Ideal Binary Nucleation Theory

In the two previous approaches, it was assumed that the mixture could be treated as an ideal mixture. In the following approach, non-ideality of the gases is introduced. By introducing the enhancement factor $f_e$, non-ideality of the vapor monomer density is taken into account. The enhancement factor is a direct measure of the deviation of ideal gas behaviour. It represents the increase of the partial saturated vapour pressure with respect to the pure vapour state.

When evaluating monomer densities, the compressibility of the gas phase must be taken into account. It is defined as $Z = p/(\rho k_B T)$, where $\rho$ is the total molar density of the mixture. For small vapor fractions, the compressibility factor of the mixture is with a high degree of precision equal to the compressibility of the carrier gas, this is the case for the n-nonane-methane mixture under consideration.

This finally gives for the equilibrium monomer number density [11]

$$\rho_{1,0}^{eq} = \rho_1^{eq} = \frac{f_e p^s}{Z k_B T},$$
(6.7)

In appendix A, expressions for evaluating $f_e$ and $Z$ can be found. The enhancement factor as well as the compressibility are dependent on the pressure, so that additional pressure dependency enters the binary nucleation expression. The numerical calculations using the non-ideal full binary nucleation theory (using mixing terms) in the case of a n-nonane-methane mixture can be seen in Fig. 6.4. For the surface tension, the pure nonane surface tension is used at corresponding conditions.

As can be seen in this figure, non-ideality plays a more important role at higher pressures,
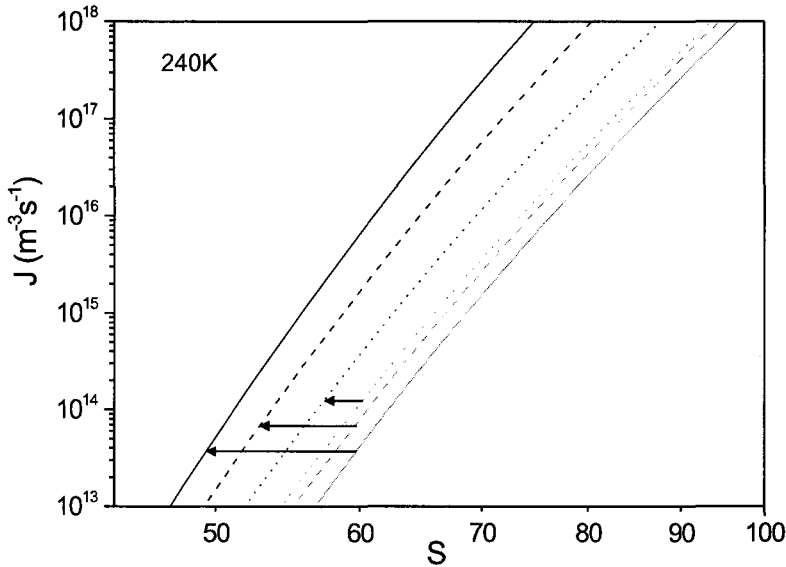


Figure 6.4: *Theoretical calculations for nucleation of n-nonane in methane at 240K at pressures of 10 bar, (dotted line), 25 bar, (dash-dotted line) and 40 bar, (dashed line) using binary theory, ideal gas assumption curves are colored grey, non-ideal curves are black. For the surface tension, the pure nonane surface tension is used at corresponding conditions. Entropic mixing terms are included into the model.*

as the effect of non-ideality increases with pressure. Non-ideality causes an increase of the nucleation rates compared to ideal behaviour. Due to the addition of non-ideality in the model, the pressure trend is reversed in comparison to the ideal nucleation behaviour. High pressures result, under these approximations, into higher nucleation rates. Still the theoretical pressure effect is not comparable to the effect observed in experiments. Theoretical

nucleation rates are very small compared to the experimental obtained rates. Non-ideality of the gases was used in this case, as well as entropic mixing terms. For the surface tension, the pure nonane surface tension was used at corresponding conditions.

### 6.1.4   Langmuir Surface Tension Correction

The surface tension of clusters plays a dominant role in nucleation behaviour, it controls the energy barrier for nucleation. Therefore it is essential to account for the effect of carrier gas pressure on the surface tension. The decrease of surface tension is generally ascribed to adsorption of the supercritical carrier gas. The following expression can be formulated for pressure dependency of surface tension

$$\left(\frac{\partial \sigma}{\partial p}\right) = -c_2^s v_2^g, \tag{6.8}$$

which means that the the surface tension is equal to minus the concentration of carrier gas molecules at the liquid phase surface times the molecular volume of carrier gas molecules in the gas phase. For the carrier gas surface concentration $c_2^s = n_a \vartheta$ can be used, where $n_a$ is the number of adsorption sites per unit area and $\vartheta$ is the surface coverage. According to the simple Langmuir adsorption model, valid up to coverages of about 30%, it can be expressed as

$$\vartheta = \frac{p}{p + p_L}, \tag{6.9}$$

where $p_L$ is the Langmuir reference pressure. From a simple statistical-mechanical model assuming discrete adsorption sites, it reads,

$$p_L = \left(\frac{m k_B T}{2\pi\hbar^2}\right)^{3/2} k_B T \exp\left(-\frac{E_a}{k_B T}\right), \tag{6.10}$$

in which $m$ is the molar mass of the adsorbing gas and $E_a$ is the adsorption energy per molecule. For the molecular volume in the gaseous phase the ideal gas law is used $v_2^g = k_B T/p$.
Substituting these assumptions into Eq. (6.8) gives

$$\left(\frac{\partial \sigma}{\partial p}\right) = -\frac{n_a k_B T}{p + p_L}, \tag{6.11}$$

which can be integrated to

$$\sigma(p) = \sigma_0 - n_a k_B T \ln\left(\frac{p + p_L}{p_L}\right). \tag{6.12}$$

Here $\sigma_0$ is the surface tension of the pure substance. Pressure $p$ is formally the carrier gas pressure, but it can always be taken equal to the total pressure. The number of adsorption

sites per unite area $n_a$ can be estimated with $n_a \approx 6 \cdot 10^{18} m^{-2}$, which is the inverse of the molecular area which is for most gases near $1.6 \cdot 10^{-19} m^2$ per molecule. The Langmuir pressure $p_L$ can be found by fitting Eq. (6.12) to experimental data [12]. Results of this fit can be seen in Fig. 6.5 [1]. For the n-nonane-methane mixture it can be estimated (in bar) using [1]

$$p_L(T) = 258.8 - 2.731T + 7.781 \cdot 10^{-3} T^2. \tag{6.13}$$

The results using Langmuir correction are displayed in Fig. 6.6 together with the exper-
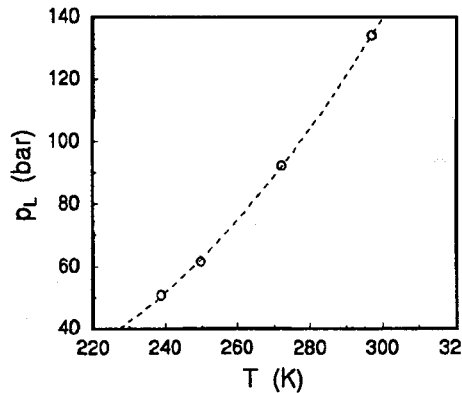


Figure 6.5: *Values of the Langmuir pressure $p_L$ in Eq. (6.13), obtained from fitting to experimental data for n-nonane-methane [12][1].*

imental results. Theoretical results are in the range of experimental data. For the lower pressures the slope of nucleation rates are well predicted. The decreasing slope with increasing pressure is not predicted.

## 6.1.5   Composition Dependent Surface Tension

In the previous section, Langmuir surface tension correction could not describe the decreasing slope with increasing pressure as is observed in experiments (Fig. 6.6). Surface tensions as a function of pressure in n-nonane-methane mixtures were measured by Deam and Maddox [12]. They used a a pressurized pending drop cell method. The Langmuir pressure has been fitted to the experimental data resulting in the fit of Eq.(6.13). The question is whether this fit from experiments on macroscopic droplets can be adapted to describe the surface tension of clusters that have the size of the critical cluster. From the previous section it appears that this approach is not valid for small clusters.

In the previous sections the surface tension was taken constant during the double summation in binary nucleation theory. This means that the surface tension was treated as a constant for all cluster-compositions summed over. In the Langmuir theory, it is clearly
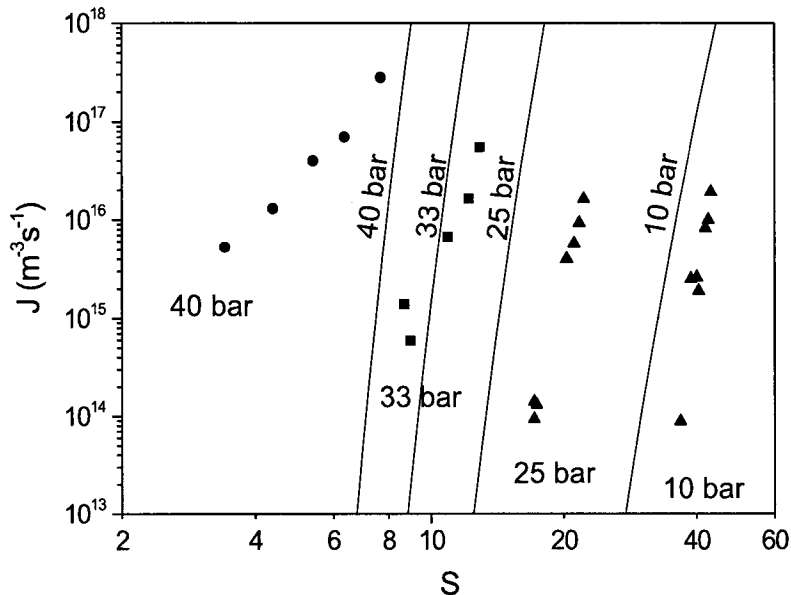
Figure 6.6: *Theoretical calculations for nucleation of n-nonane in methane at 240K at pressures of 10 bar, 25 bar, 33 bar and 40 bar using full Langmuir binary nucleation theory, in comparison with experimental data. Non-ideality and mixing terms are taken into account.*

stated that adsorption of methane molecules at the cluster surface leads to a decrease of surface tension. So a constant surface tension seems not to be logical, while conducting the full summations over vapor-gas space.

The next approach is to use a composition dependent surface tension inspired on the parachor method, in which the surface tension is obtained from [1]

$$\sigma^{1/4} = \sum_i P_i \left( \frac{x_i}{V^l} - \frac{y_i}{V^v} \right). \tag{6.14}$$

Here, $P_i$ is the parachor of component $i$ fitted to experimental values. The second term in this equation is neglected, as the molar volume in the gas phase $V^g$, is much larger than the molar volume in the liquid phase $V^l$. The sum in Eq.(6.14) can be extended and rewritten as

$$\sigma = \sigma_L \left( \frac{1 + \kappa \frac{n_g}{n_v}}{1 + \nu \frac{n_g}{n_v}} \right)^4, \tag{6.15}$$

using $V^l = n_v + \nu n_g$, and $\kappa$ as the ratio of parachors $(\kappa = P_{C1}/P_{C9})$. For numerical calculations, the Langmuir corrected surface tension was used as a reference surface tension. It

is easy to see that this parachor surface tension is dependent on composition. In a first approximation, $\nu$ is given the constant value of $1/9$ and $\kappa$ is varied. In literature experimental values for the parachor values can be found, but these are only valid for flat surfaces, in this approach it is chosen to vary this fraction in order to study the effect on nucleation rates. Binary nucleation theory was used and evaluated at $240K$ and 40 bar, using the parachor surface tension. Mixing terms are neglected, as methane molecules are adsorbed at the cluster surface and are not uniformly dispersed in the cluster.

The results for these calculations together with the experimental results are shown in Fig. 6.7. The composition dependence of the surface tension is strongly dependent on the value of $\kappa$. Decreasing $\kappa$ causes a strong increase of nucleation rates. Also a decrease in slope can be observed for lower values of $\kappa$. But the slope for these lower $\kappa$ values is still much steeper than the experimentally found slope.
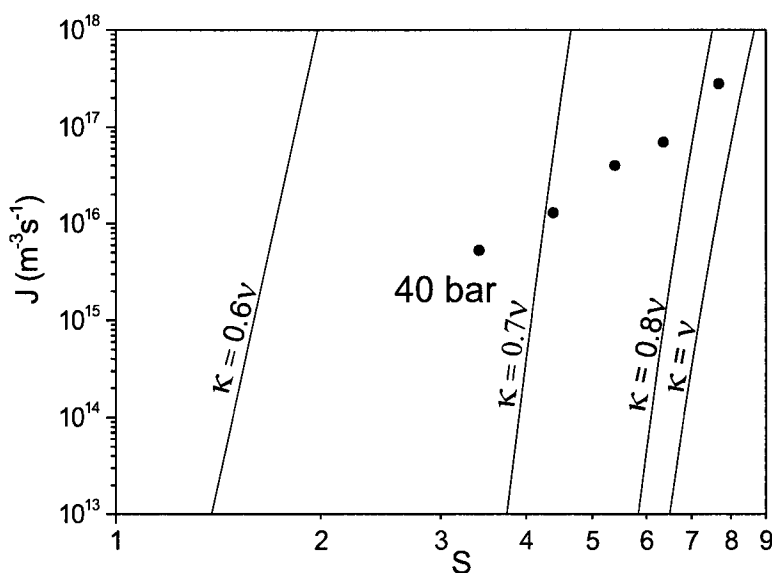


Figure 6.7: *Theoretical calculations for nucleation of n-nonane in methane at 240K at a pressure of 40 bar using a parachor corrected surface tension with different values for $\kappa$, the ratio of the parachors. Circles are experimental data points.*

## 6.2   Discussion

Instead of using the full binary theory, Eq. (6.2), also unary theory can be applied, Eq. (6.1). The classical unary theory can be adapted to describe the influence of carrier gas pressure in a similar way as binary theory (accept for introduction of the entropic mixing terms). We will refer to this adapted unary theory as quasi unary theory. Quasi unary theory takes into account non-ideality of gases (using Eq. (6.7)), and Langmuir surface tension pressure correction, Eq. (6.12). The advantage of using quasi unary theory instead of binary theory is the analytical solution of the quasi unary theory, this saves a lot of calculation time. Calculations using quasi unary theory are compared to binary theory and experiments in Fig. 6.8.

As can be seen in this figure, there is almost no difference in results between quasi unary
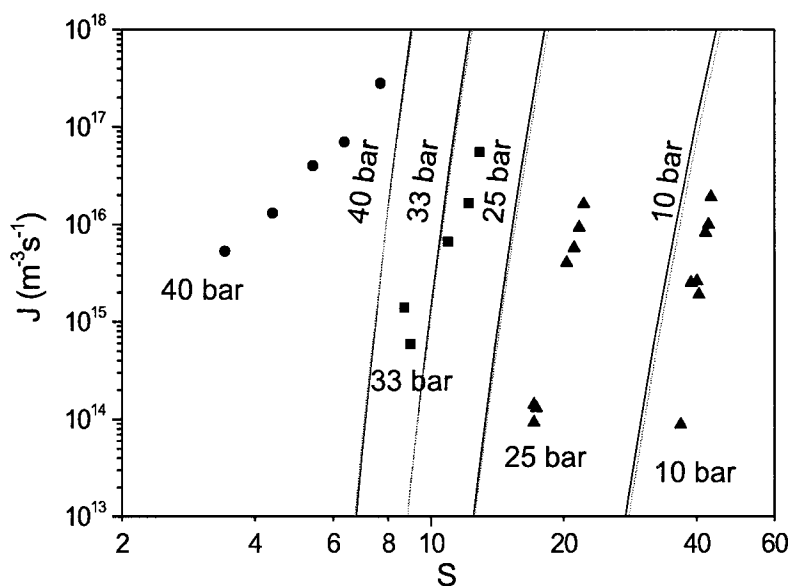


Figure 6.8:  *Theoretical calculations for nucleation of n-nonane in methane at 240K at pressures of 10 bar, 25 bar, 33 bar and 40 bar using full binary nucleation theory (black curves)and quasi unary theory (grey curves), in comparison with experimental data.*

and full binary theory. At this stage it is therefore more convenient to use quasi unary theory instead of full binary theory, as quasi unary theory has an analytical solution.

Both binary and full unary theory are not able to predict nucleation behaviour at high pressures. The Langmuir corrected surface tension appears to be invalid at these pressures.

In Fig. 6.9, iso-$\theta$ contour lines are displayed together with the experimental results at 40 bar and 240K.

From this figure it becomes clear that the surface tension (using binary theory) does not
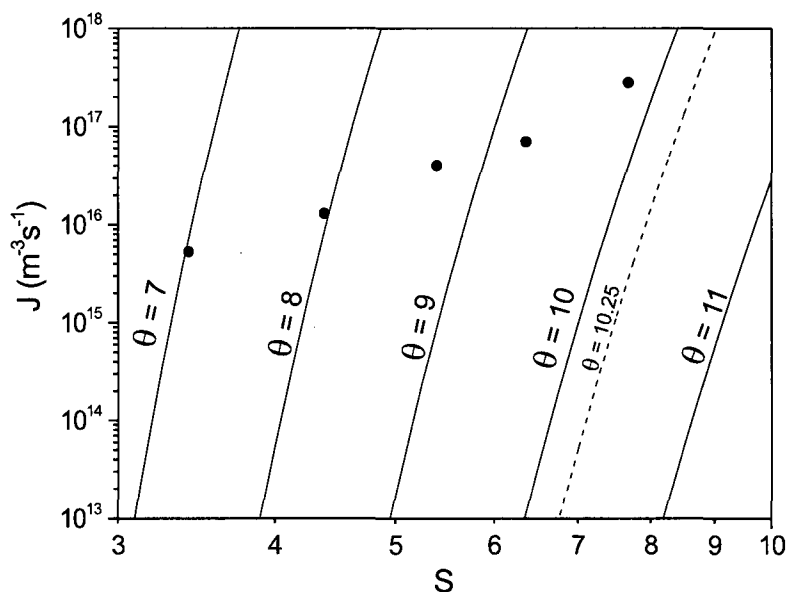


Figure 6.9: *Iso-$\theta$ contour lines for nucleation of n-nonane in methane at 240K and 40 bar. Squares are experimental results. Dashed line is the predicted theoretical curve.*

have a constant value in the experimental range of supersaturation values. Langmuir surface tension correction apparently does not work at these conditions. Overall experimental nucleation rates are several orders of magnitude higher than theoretical ones, this is especially the case for low supersaturation.

In the derivation leading to the final Langmuir model, Eq. (6.9) was used, which is only valid for coverages up to 30%, the question is whether this is the case at 40 bar and 240K. Equilibrium models show that the mole fraction of methane in the bulk liquid phase at these conditions is equal to about 25%. The adsorption of methane molecules at the surface of the cluster is likely to be above 25%. So the validity of the Langmuir correction at these conditions is questionable.

The Langmuir pressure has been fitted to experimental data of surface tensions for several temperature. Surface tensions as function of pressure in n-nonane-methane were measured by Deam and Maddox [12]using a pressurized pending drop cell method. These are measurements performed on macroscopic droplets. The question is whether the measured

surface tension of macroscopic droplets is valid for the microscopic critical clusters during nucleation. Langmuir surface tension correction is thus a very rough method in calculating surface tensions, but it is at the moment the best method available.

In the binary calculations the surface tension was kept constant for all cluster sizes and compositions. In the previous section a first attempt was made to use a surface tension dependent on composition. As can be seen in Fig. 6.7, a variable surface tension can have an influence on the slope of the theoretical curve. More attention has to be payed in order to develop a new variable surface tension, depending on size and composition. This in order to have a more realistic surface tension model.

# Chapter 7

# Experimental Results

## 7.1 Introduction

In this chapter results are presented regarding two series of experiments performed using the wave tube expansion method described in the chapter on wave tube experiments. In these experiments, nucleation of the ternary methane-propane-n-nonane mixture was studied at nucleation conditions of approximately $235K$, $10\,bar$ and a propane fraction around 1%. Another series of experiments were conducted with the same conditions. Something went wrong with the mixture preparation of these experiments, in Appendix D, these series of experiments are discussed.

The ternary mixture was prepared using the setup as depicted in Fig.4.3 in the saturators. The nucleating component in the experiments is n-nonane. The binary mixture of methane and propane is acquired from Hoek Loos BV. Equilibrium calculations were performed using the PE2000 program. The RKS equation of state was selected for these calculations.

In the next section the experiment $09jul05\,002$ will be used to illustrate the procedure to extract the nucleation results from the experimental data.

## 7.2 Experiment $09jul05\,002$

Experiment $09jul05\,002$ belongs to the second series of nucleation experiments of the methane-propane-n-nonane mixture. Table 7.1 lists the initial conditions of the experiment. This data is necessary in the subsequent analysis of the experimental results.

From the mixture preparation data, the initial mixture composition at the beginning of the nucleation experiment can be calculated. The methane/propane flow through the saturators is saturated with n-nonane vapour, the fraction of n-nonane in this flow can be calculated using an appropriate equation of state. In the experiments the RKS equation

| Mixture prep. | |
|---|---|
| $T_{sat}(K)$ | 290.63 |
| $P_{sat}(bar)$ | 30.00 |
| $Q_1(nl/min)$ | 0.0000 |
| $Q_2(nl/min)$ | 2.0475 |
| $Y_{C3} \cdot 10^3$ | 10.0 |
| Nucl. cond. | |
| $T_0(K)$ | 294.45 |
| $P_0(bar)$ | 24.85 |

Table 7.1: *Initial experimental conditions for nucleation experiment* $09jul05\,002$ *for the nucleation of n-nonane in the ternary methane-propane-n-nonane mixture.*

| | |
|---|---|
| $y_{C1,mix}$ | $9.897 \cdot 10^{-1}$ |
| $y_{C3,mix}$ | $9.991 \cdot 10^{-3}$ |
| $y_{C9,mix}$ | $3.090 \cdot 10^{-4}$ |

Table 7.2: *Initial mixture composition in the high pressure section of the shock tube at the beginning of nucleation experiment* $09jul05\,002$ *for the nucleation of n-nonane in the ternary methane-propane-n-nonane mixture.*

of state was selected. The equilibrium vapour fraction of n-nonane and propane in the saturators ($y_{C3,sat}^{eq}$ and $y_{C9,sat}^{eq}$) is calculated at the conditions of $T_{sat}$, $P_{sat}$ and $Y_{C3}/1 - Y_{C3}$ (which has to be constant according to Eq. (4.2). After this calculation the composition of flow $Q_2$ is known. The final mixture composition can now be determined using

$$y_{C3,mix} = \frac{Q_1 Y_{C3} + q_2 y_{C3,sat}^{eq}}{Q_1 + q_2} \tag{7.1}$$

and

$$y_{C9,mix} = \frac{q_2 y_{C9,sat}^{eq}}{Q_1 + q_2}, \tag{7.2}$$

where

$$q_2 = Q_2 \frac{Y_{C3}}{y_{C3,sat}^{eq}}. \tag{7.3}$$

Now the initial mixture composition in the high pressure section of the shock tube at the beginning of the nucleation experiment is known. For experiment $09jul05\,002$ the composition can be found in Table 7.2.

During the nucleation experiment, three signals are obtained, the pressure curve, the $90°$-scattering signal and the transmitted intensity signal. From these three signals all the nucleation and droplet growth data can be extracted.

### 7.2.1 The Pressure Signal

The pressure curve of experiment 09$jul$05 002 is shown in Fig. 7.1. The pressure dip is
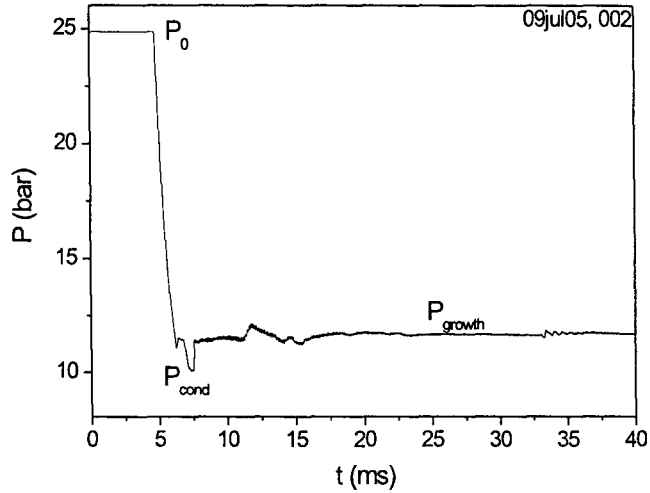


Figure 7.1: *Pressure signal of nucleation experiment* 09$jul$05 002 *of the methane-propane-n-nonane mixture.*

clearly visible. At this stage all the critical clusters are formed. The pressure in the dip ($P_{cond}$) is determined from this graph. The dip is followed by a pressure plateau where the droplet growth takes place, the average pressure during droplet growth ($P_{growth}$) can also be obtained from this graph. The corresponding temperatures during nucleation ($T_{cond}$) and droplet growth ($T_{growth}$) can be calculated using an appropriate equation of state (RKS was used) and knowing the initial pressure $P_0$ and temperature $T_0$. The pressures and temperatures for experiment 09$jul$05 002 are shown in Table 7.3.

With the values of $T_{cond}$, $P_{cond}$ and $y_{C3,mix}$ the equilibrium nonane vapour fraction $y_{C9,cond}^{eq}$ is calculated using for instance the RKS equation of state. This equilibrium value at the nucleation condition is necessary to determine the supersaturation of n-nonane in the mixture. The supersaturation of nonane is then determined by:

$$S_{C9,exp} = \frac{y_{C9,mix}}{y_{C9,cond}^{eq}}. \tag{7.4}$$

For experiment 09$jul$05 002, $y_{C9,cond}^{eq} = 5.267 \cdot 10^{-6}$ and the supersaturation is equal to $S_{C9,exp} = 58.67$.

From Fig. 7.1 the pulse duration can also be obtained, this value is necessary for determining the nucleation rate given by Eq. (4.1). For experiment 09$jul$05 002, the pulse duration

| | |
|---|---|
| $P_0(bar)$ | 24.85 |
| $T_0(K)$ | 294.85 |
| $P_{cond}(bar)$ | 10.11 |
| $T_{cond}(K)$ | 236.10 |
| $P_{growth}(bar)$ | 11.63 |
| $T_{growth}(K)$ | 244.17 |

Table 7.3: *Pressures and temperatures obtained from the pressure profile (Fig. 7.1) of nucleation experiment 09jul05 002 of the methane-propane-n-nonane mixture. Corresponding temperatures were calculated using the RKS equation of state.*

$\Delta t$ is equal to $0.41ms$.

## 7.2.2   The 90-Degrees-Scattering Signal

During nucleation experiment $09jul05\,002$ the scattered intensity of the growing droplets was obtained. The 90°-scattering signal is shown in Fig. 7.2.

Several Mie-extrema can be distinguished, they are numbered according to Mie theory.
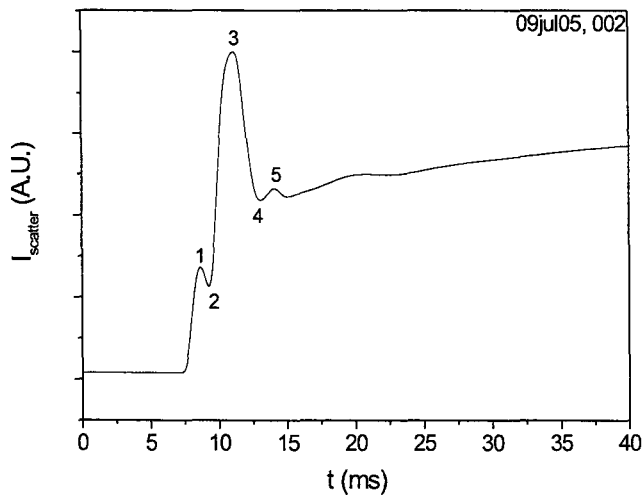


Figure 7.2: *The 90°-scattering signal of nucleation experiment 09jul05 002 of the methane-propane-n-nonane mixture. Corresponding extrema described by Mie theory are numbered.*

Each extremum corresponds to a specific droplet size.  This way a time resolved radius

curve can be obtained. One extra point can be added to this curve, at the starting point of the droplet growth the radius is equal to zero. For the starting point of droplet growth the time corresponding to the center of the pressure pulse is taken. In Fig. 7.3 the radius squared is plotted against time. The slope of the linear fit is equal to the surface growth rate of the droplets. In this experiment it is equal to $2.3 \pm 0.2 \cdot 10^{-2} \mu m^2 m s^{-1}$.
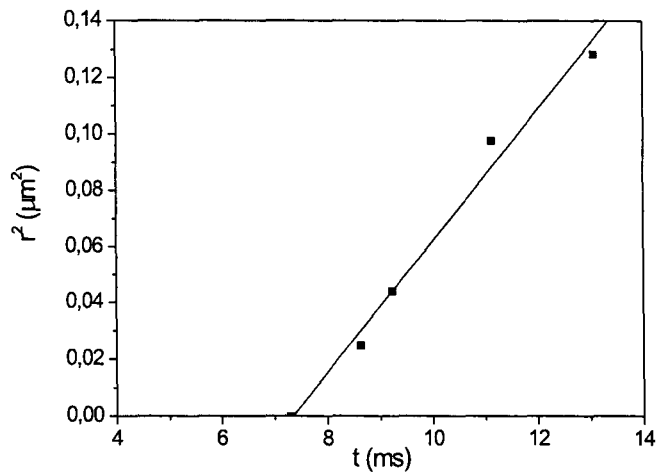


Figure 7.3: *The droplet radius squared of nucleation experiment* 09*jul*05 002 *of the growing droplets, points correspond to the Mie peaks obtained from Fig. 7.2 and Mie theory. The slope of the linear fit is the surface growth rate which is equal to* $2.3 \pm 0.2 \cdot 10^{-2} \mu m^2 m s^{-1}$ *for this experiment. The point with a droplet radius of* 0 *corresponds to the center of the pressure pulse.*

### 7.2.3 The Transmitted Intensity Signal

The transmitted intensity signal of experiment 09*jul*05 002 is displayed in Fig. 7.4. The transmitted intensity is governed by Lambert-Beer's law Eq. (4.5). As discussed in the section on light extinction in the chapter on the experimental procedure, the extinction coefficient depends on the extinction efficiency which can be calculated from Mie theory. For the Mie extrema points in Fig. 7.2 this efficiency is calculated. With this efficiency and the transmitted light intensity, the number density $n_d$ is derived from Eq. (4.5) and Eq. (4.6). In the case of experiment 09*jul*05 002 the number density $n_d$ is equal to $2.6 \pm 0.3 \cdot 10^{13} m^{-3}$. Together with the pulse duration of $0.41 ms$, the nucleation rate is $J = 6.5 \pm 0.7 \cdot 10^{16} m^{-3} s^{-1}$.
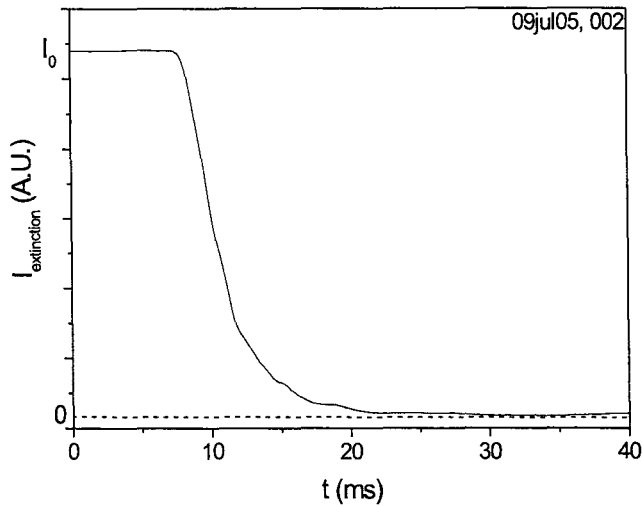
Figure 7.4: *The transmitted intensity signal of nucleation experiment* $09jul05\,002$ *of the methane-propane-n-nonane mixture.*

## 7.3   Experimental Series

The procedure as discussed in the previous section was repeated for each experiment. Two series of experiments were performed on nucleation of the methane-propane-n-nonane mixture at a nucleation temperature of approximately $T_{cond} \approx 235K$ and a nucleation pressure of $P_{cond} \approx 10bar$. The amount of propane in the mixture was in all experiments approximately around 1%. All the obtained data from the experiments can be found in Appendix C.

From this data the surface growth curve can be produced. This curve displays the rate of increase of the surface of the droplet in time, as a function of the fraction of supersaturated vapour in the gas mixture, governed by Eq. (3.20) for diffusion controlled droplet growth. The surface growth curve for the two series of experiments is displayed in Fig. 7.5. As can be seen from this graph, there is quite some scatter in surface growth rate data but overall the results seem to be consistent with diffusion controlled droplet growth theory.

For producing the nucleation rate plot the supersaturation can now be calculated using:

$$S = \frac{y_{C9,mix}}{y_{C9,cond}^{eq}}. \tag{7.5}$$

Each experiment is performed at slightly different nucleation conditions. The scatter in temperature is corrected by the following equation, in which it is assumed that classical
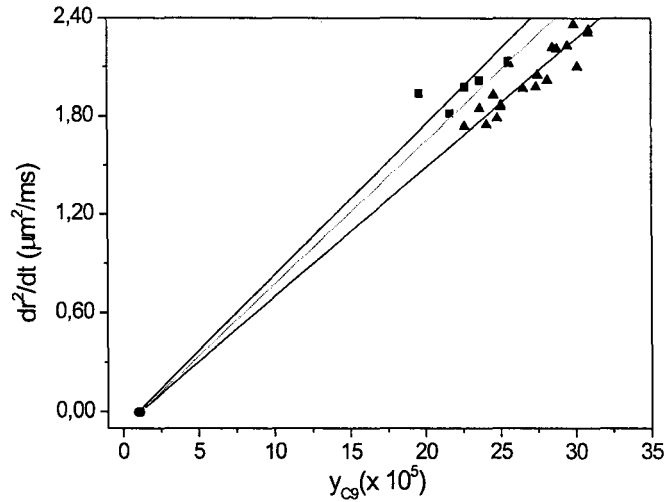
Figure 7.5: *Surface growth rate versus n-nonane vapour fraction for nucleation experiments of the ternary mixture methane-propane-nonane. Squares are experimental results from series 1, triangles series 2. The circles are the equilibrium n-nonane vapour fraction at the average temperature, pressure and propane fraction of each series. The grey lines are theoretical curves calculated using Wilke and Lee method for average temperature and pressure of each series, the black lines are linear fits for each series. Data can be found in appendix C.*

nucleation theory predicts the right temperature and supersaturation trends for sufficiently small ranges

$$S_{corr} = S + \left(\frac{\partial S}{\partial T}\right)_J \delta T = S + \frac{3}{2}\frac{S \ln S}{T}\left[1 - \frac{T}{\sigma}\frac{\mathrm{d}\sigma}{\mathrm{d}T}\right](T - T_{aim}). \qquad (7.6)$$

Here $T_{aim}$ is the desired nucleation temperature, which for these experiments is set to the average nucleation temperature. For the two series of experiments the results are displayed in Fig. 7.6. As can be seen in this figure, the nucleation rates show appreciable scatter, but a trend is clearly visible.

An attempt is made to reduce the scatter in the nucleation rates caused by the inaccuracy in calculating the nonane fraction in the mixture. The idea is that the droplet growth rate is accurately known, and that the error in the composition of the mixture is responsible for the scatter in the surface growth rates. The, the surface growth rates can be used to correct the values for the components. The correction is performed by adjusting the nonane fraction in the surface growth curve in order to match to the average rate of each series. As the droplet growth conditions in the series is somewhat different, each experiment is corrected to the average value of its own series. It is assumed that all diffusion processes

Figure 7.6:  *Nucleation rate versus supersaturation for nucleation experiments of the methane-propane-nonane mixture, the propane vapour fraction is approximately 1%. Squares are experimental results from series 1 and triangles of series 2.  The supersaturation is temperature corrected to the average temperature of the experiments.  Data can be found in appendix C.*

are similar for each series and thus, the diffusion coefficient should be approximately the same.  So every experiment in one series is attributed with the same diffusion coefficient, leading to a new value for the nonane fraction and thus to a different supersaturation value. The results for the corrected nucleation rate can be seen in Fig. 7.7.

On the average the scatter has decreased because of this correction, especially at low supersaturation values.  At high supersaturation, the scatter has slightly increased.  For the nucleation rates, the same trend is found as in Fig. 7.6.

## 7.4   Effect of Propane on Nucleation of Nonane in Methane

The experimental results of the nucleation of the methane-propane-nonane mixture can be compared to the nucleation of the binary methane-nonane mixture at the same conditions to examine the effect of adding 1% of propane to the mixture.  In Fig. 7.8 experimental nucleation rates of the binary mixture and of the ternary mixture are displayed.  For the ternary mixture the nonane fraction is corrected using the average diffusion coefficient of each series, as also was done in Fig. 7.7.
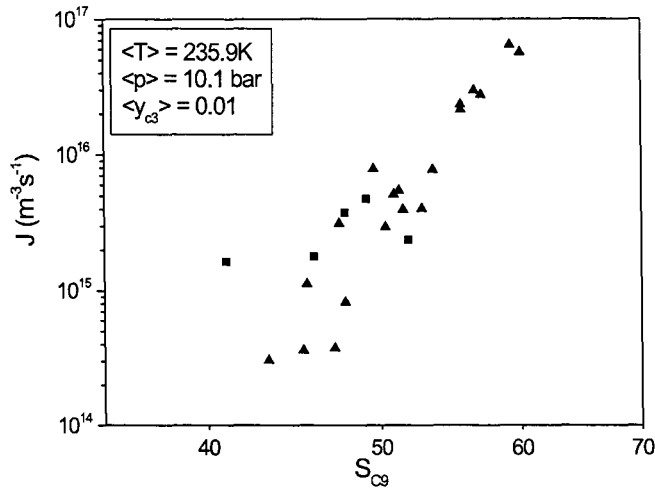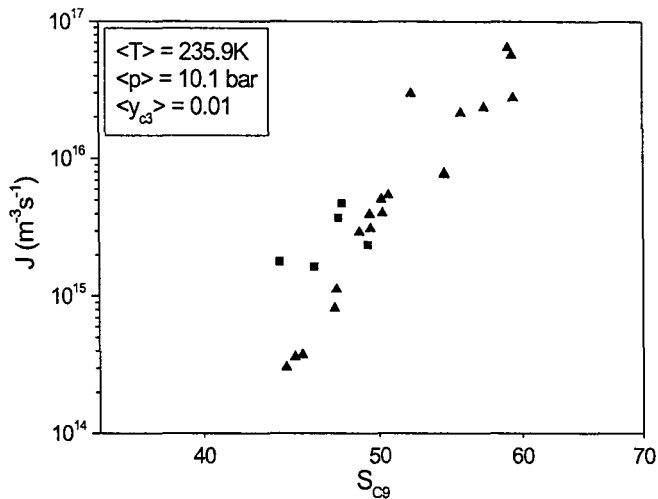
Figure 7.7: *Nucleation rate versus supersaturation for nucleation experiments of the methane-propane-nonane mixture, the propane vapour fraction is approximately 1%. The nonane vapour fraction is corrected on the basis of the surface growth rates. Squares are experimental results from series 1 and triangles of series 2. The supersaturation is temperature corrected to the average temperature of the experiments.*

As can be seen in this image, there is no significant difference between the nucleation in the binary and the ternary mixture at these conditions ($T_{cond} \approx 235K$, $P_{cond} \approx 10bar$). The effect of propane for this case is hardly visible.

A possible difference in nucleation behaviour between the binary and the ternary mixture, can be caused by a difference of the surface tension in the droplet. The addition of propane to the binary methane-nonane mixture could influence the droplet surface tension as propane will change the composition of the droplet. With the use of the parachor method, the theoretical difference between the surface tensions of the methane-nonane mixture and the methane-propane-nonane mixture can be estimated for the given experimental conditions. The parachor equation is given by Eq.(6.14):

$$\sigma^{1/4} = \sum_i P_i \left( \frac{x_i}{V^l} - \frac{y_i}{V^v} \right). \qquad (7.7)$$

Here, $P_i$ is the parachor of component $i$ fitted to experimental values. The second term in this equation is neglected, as the molar volume in the gas phase $V^g$, is much larger than the molar volume in the liquid phase $V^l$.

For the three components, the theoretical values for the parachors can be found in literature. The parachors are, $P_{C1} = 81.0$ [12], $P_{C3} = 151.9$ [13] and $P_{C9} = 387.6$ [12]. For
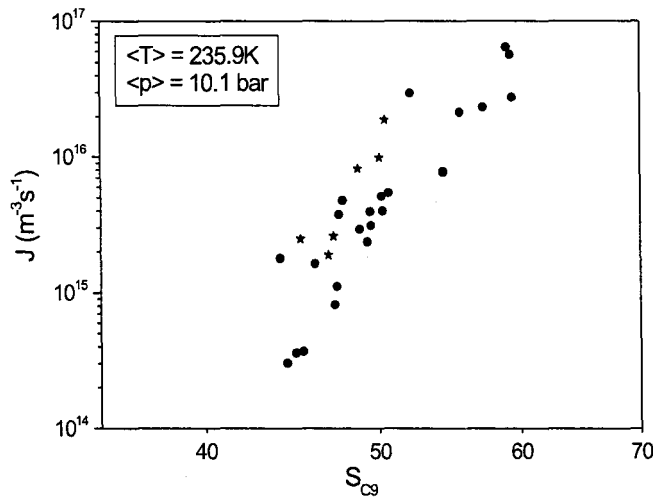
Figure 7.8: *Nucleation rate versus supersaturation for nucleation experiments of the binary methane-nonane mixture (stars)and the ternary methane-propane-nonane mixture (circles) and. Experiments of the binary mixture were performed by Luijten [1]. The propane vapour fraction in the ternary mixture is approximately 1%. The nonane vapour fraction of the ternary mixture is corrected by the average diffusion coefficient of each series. The supersaturation is temperature corrected to the average temperature of the experiments.*

| Mixture | $x_{C3}^{eq}$ | $x_{C9}^{eq}$ | $\rho^l(mol/l)$ |
|---|---|---|---|
| $CH_4 - C_9H_{20}$ | 0 | 0.9217 | 5.218 |
| $CH_4 - C_3H_8 - C_9H_{20}$ | 0.0687 | 0.8532 | 5.459 |

Table 7.4: *Liquid equilibrium conditions for the binary and ternary mixture at $T_{cond} = 235.9K$ and $P_{cond} = 10.1bar$, for the ternary mixture $y_{C3}^{eq} = 1\%$, RKS equation of state was used.*

the experimental conditions, the equilibrium compositions of the liquid are calculated and sepcified in Table 7.4 With this data the surface tension is calculated, resulting in

$$\sigma_{tern} = 0.998\sigma_{bin}. \tag{7.8}$$

So there is only a minor difference in surface tension between the two mixtures. The effect of this difference on nucleation rates can be estimated using ICCT, Eq.(2.25). The result is:

$$J_{tern} = 1.004J_{bin}. \tag{7.9}$$

So the effect of the difference between the surface tension of the binary and ternary mixture is very small and not detectable in nucleation experiments.

# Chapter 8

# Conclusions and Recommendations

## 8.1  Numerical Nucleation Calculations

This report discusses many aspects of nucleation study. First classical nucleation theory was treated as well as a simplified binary nucleation theory. The question was whether the "simple" ICCT would predict the same nucleation behaviour as the extended binary theory using the full double summation over the gas and vapour molecules, for the nucleation of nonane in methane. It was concluded that with the present binary model, using the Langmuir approach for calculating the droplet surface tension, there is no significant difference in the prediction of nucleation behaviour between ICCT and the binary theory.

ICCT and binary theory fail in predicting nucleation behaviour at high nucleation pressures. This is probably caused by the model used for the surface tension. This model assumes that each cluster, independent of size and composition has the same surface tension at constant nucleation pressure and temperature. Since the Langmuir surface tension model is derived from experimental flat liquid surface data, it is not very likely that this data also holds for microscopic clusters.

At this moment, it is most convenient to use ICCT for the prediction of nucleation rates as it is a simple and efficient theory compared to the time consuming double summation in the binary nucleation model.

A study on surface tension for microscopic clusters would be necessary for improvement of the nucleation theory. This model should incorporate size and composition dependency of the surface tension. When such a model is developed, the binary double summation nucleation model should probably be used for calculating nucleation rates.

## 8.2  Nucleation Experiments

This report discusses the results from nucleation experiments performed with a methane-propane-nonane mixture, in which nonane is supersaturated and is thus the nucleating component. In order to fully understand the principle of nucleation experiments, some theory had to be studied. This theoretical study has also been presented in this report. This includes a chapter on droplet growth and one on wave tube experiments. An equilibrium model was constructed using the PE2000 program for this mixture to make equilibrium calculations easier and faster. Another model was made for the ternary mixture, methane-carbondioxide-nonane, as it was needed for other experiments not treated in this report.

For all phase equilibrium calculations the RKS equation of state was used. The accuracy of this equation of state determines for a large portion the accuracy of nucleation experiments, as it is used to calculate temperatures and mixture compositions. This introduces systematic errors, and continuous effort and research should be put into improving the accuracy of equilibrium calculations.

Experiments were performed on the methane-propane-nonane mixture, at nucleation conditions of approximately $235K$ and $10bar$ with a propane vapour fraction around 1%. Results showed no significant difference in nucleation behaviour between the nucleation of the methane-propane-nonane mixture and the methane-nonane mixture, see Fig. 7.8. This indicates that at given nucleation conditions, the influence on nucleation of nonane in methane of propane is negligible. This also follows from nucleation theory using the Parachor method to compare surface tensions for both cases.

In order to improve the nucleation data, an attempt was made to correcting the nonane vapour fraction with the use of droplet growth theory. Each experiment was corrected using the average diffusion coefficient of the experimental series and subsequently calculating the corresponding nonane vapour fraction using the droplet surface growth rate. This reduced the scatter in the nucleation rate vs. supersaturation plot.

More experiments could be performed using the methane-propane-nonane mixture, using different nucleation conditions and different propane fractions, in order to study the effect of propane on the nucleation behaviour. It would be wise to do some theoretical research prior to these experiments to examine the nucleation conditions at which an influence of propane is expected to occur.

# Bibliography

[1] C. Luijten, *Nucleation and Droplet Growth at High Pressures*. University Press Eindhoven, 1998. Eindhoven.

[2] P. Peeters, *Nucleation and Condensation in Gas-Vapor Mixtures of Alkanes and Water*. University Press Eindhoven, 2002. Eindhoven.

[3] K. Looijmans, *Homogeneous Nucleation and Droplet Growth in the Coexistence Region of n-alkane/methane Mixtures at High Pressures*. University Press Eindhoven, 1995. Eindhoven.

[4] R. Reid, J. Prausnitz, and B. Poling, *The Properties of Gases and Liquids, 4th edition*. McGraw-Hill, Inc., 1987. New York.

[5] L. Shipman and J. Kohn, "Heterogeneous phase and volumetric equilibrium in the methane-n-nonane system," *Journal of Chemical and Engineering Data*, vol. 11, 1966.

[6] J. Prausnitz, R. Lichtenthaler, and E. G. de Azevedo, *Molecular Thermodynamics of Fluid-Phase Equilibria, 2nd edition*. Prentice-Hall, 1986. New Jersey.

[7] "http://www.tu-harburg.de," *Technische Universitt Hamburg-Harburg*.

[8] D. Jennings and R. Schucker, "Comparison of high-pressure vapour-liquid equilibria of mixtures of $co_2$ or propane with nonane and $c_9$ alkylbenzenes," *Journal of Chemical and Engineering Data*, vol. 41, 1996.

[9] W.Wei, T. Brown, A. Kidnay, and E. Sloan, "Vapor + liquid equilibria for the ternary system methane + ethane + carbon dioxide at 230k and its constituent binaries at temperatures from 207 to 270k," *Journal of Chemical and Engineering Data*, vol. 40, 1995.

[10] L. Webster and A. Kidnay, "Vapor-liquid equilibria for the methane-propane-carbon dioxide systems at 230k and 270k," *Journal of Chemical and Engineering Data*, vol. 46, 2001.

[11] C. Luijten and M. van Dongen, "Nucleation at high pressure. i. theoretical considerations," *Journal of Chemical and Engineering Data*, vol. 15, 1970.

[12] J. Deam and R. Maddox, "Interfacial tension in hydrocarbon systems," *Journal of Chemical and Engineering Data*, vol. 15, 1970.

[13] C. Weinaug and D. Katz, "Surface tensions of methane-propane mixtures," *Industrial and Engineering Chemistry*, vol. 35, 1943.

# Appendix A

# Physical Properties

|  |  | n-Nonane |  |
|---|---|---|---|
| $M$ | = | 128.259 | $kg\,kmol^{-1}$ |
| $p_c$ | = | 22.9 | $bar$ |
| $T_c$ | = | 594.6 | $K$ |
| $V_c$ | = | 548 | $cm^3\,mol^{-1}$ |
| $d$ | = | 0.683 | $nm$ |
| $C_p$ | = | $-8.374 + 0.8729T - 4.823 \cdot 10^{-4}T^2$ $+1.031 \cdot 10^{-7}T^3$ | $J\,mol^{-1}\,K^{-1}$ |
| $p^s$ | = | $133.322\exp(-17.56832\ln T + 0.0152556T$ | |
| $\rho_l$ | = | $733.5 - 0.788(T - 273.15)$ $-9.689 \cdot 10^{-5}(T - 273.15)^2$ | $kg\,m^{-3}$ |
| $L$ | = | $4.944 \cdot 10^3[7.08(1 - T/T_c)^{0.354}$ $+4.873(1 - T/T_c)^{0.456}]$ | $J\,mol^{-1}$ |
| $\sigma_0$ | = | $0.02472 \cdot 10^{-5}(T - 273.15)$ | $N\,m^{-1}$ |

Table A.1: *Physical properties for n-nonane.*

**Enhancement factor for n-nonane-methane**

$$\ln(f_e) = b(T)[p - p^s(T)] + c(T)[p - p^s(T)]^2 \tag{A.1}$$

$$b(T) = 2.385 \cdot 10^{-1} - 7.26 \cdot 10^{-4}T - 1.29 \cdot 10^{-6}T^2 + 4.61 \cdot 10^{-9}T^3 \tag{A.2}$$

$$c(T) = 2.424 \cdot 10^{-2} - 2.552 \cdot 10^{-4}T + 8.985 \cdot 10^{-7}T^2 - 1.057 \cdot 10^{-9}T^3 \tag{A.3}$$

**Compressibility of methane**

$$Z = 1 + A_0 \tag{A.4}$$

65

| | | **Methane** | |
|---|---|---|---|
| $M$ | = | 16.043 | $kg\,kmol^{-1}$ |
| $p_c$ | = | 46.0 | $bar$ |
| $T_c$ | = | 190.4 | $K$ |
| $V_c$ | = | 99.2 | $cm^3\,mol^{-1}$ |
| $d$ | = | 0.3758 | $nm$ |
| $C_p$ | = | $19.25 + 5.213 \cdot 10^{-2}T + 1.197 \cdot 10^{-5}T^2$ | |
| | | $-1.132 \cdot 10^{-8}T^3$ | $J\,mol^{-1}\,K^{-1}$ |

Table A.2: *Physical properties for methane.*

$$A_0 = \sum_{i=1}^{10} \sum_{j=0}^{7} b_{ij} \frac{\rho_r^i}{T_r^j} \tag{A.5}$$

$$\rho_r = \frac{\rho}{\rho_c} \tag{A.6}$$

$$T_r = \frac{T}{T_c} \tag{A.7}$$

| | | |
|---|---|---|
| $b_{10} = 0.5365574$ | $b_{40} = 0.2431204 \cdot 10^{-1}$ | $b_{73} = 0.2985520 \cdot 10^{-2}$ |
| $b_{11} = -0.1671289 \cdot 10^1$ | $b_{41} = 0.3478417$ | |
| $b_{12} = 0.1704335 \cdot 10^1$ | $b_{42} = 0.3587548 \cdot 10^{-1}$ | $b_{80} = 0.3030236 \cdot 10^{-1}$ |
| $b_{13} = -0.4003982 \cdot 10^1$ | $b_{42} = 0.3587548 \cdot 10^{-1}$ | $b_{81} = -0.1014545 \cdot 10^{-2}$ |
| $b_{14} = 0.3491415 \cdot 10^1$ | $b_{43} = 0.2945131$ | $b_{82} = -0.1847890 \cdot 10^{-1}$ |
| $b_{15} = -0.1332024 \cdot 10^1$ | $b_{44} = 0.1565847 \cdot 10^{-1}$ | $b_{83} = 0.3250667 \cdot 10^{-2}$ |
| $b_{16} = 0.5440249 \cdot 10^{-1}$ | $b_{45} = -0.4257759$ | |
| $b_{17} = 0.5211075 \cdot 10^{-1}$ | | $b_{90} = -0.6183691 \cdot 10^{-2}$ |
| | $b_{50} = 0.1779964$ | $b_{91} = 0.6643026 \cdot 10^{-2}$ |
| $b_{20} = 0.7187518 \cdot 10^{-1}$ | $b_{51} = -0.2754465 \cdot 10^{-1}$ | $b_{92} = 0.9014904 \cdot 10^{-3}$ |
| $b_{21} = 0.5481658$ | $b_{52} = -0.5843797$ | $b_{93} = -0.8454372 \cdot 10^{-3}$ |
| $b_{22} = -0.1932578 \cdot 10^1$ | $b_{53} = 0.2273617$ | |
| $b_{23} = 0.4295984 \cdot 10^1$ | $b_{54} = -0.7393567 \cdot 10^{-1}$ | $b_{100} = 0.6100390 \cdot 10^{-3}$ |
| $b_{24} = -0.3969273 \cdot 10^1$ | $b_{55} = 0.1461452 \cdot 10^{-1}$ | $b_{101} = -0.1371245 \cdot 10^{-2}$ |
| $b_{25} = 0.1944849 \cdot 10^1$ | | $b_{102} = 0.6833971 \cdot 10^{-3}$ |
| $b_{26} = -0.5923964$ | $b_{60} = 0.1650834$ | |
| | $b_{61} = 0.1337959$ | |
| $b_{30} = 0.4802716 \cdot 10^{-1}$ | $b_{62} = 0.1158357$ | |
| $b_{31} = 0.1443345$ | $b_{63} = -0.1025381$ | |
| $b_{32} = -0.1249822 \cdot 10^1$ | $b_{64} = 0.7468426 \cdot 10^{-1}$ | |
| $b_{33} = 0.1618220 \cdot 10^1$ | | |
| $b_{34} = -0.1690813 \cdot 10^1$ | $b_{70} = -0.8863694 \cdot 10^{-1}$ | |
| $b_{35} = 0.1154217 \cdot 10^1$ | $b_{71} = -0.6837762 \cdot 10^{-1}$ | |
| $b_{36} = 0.9352795 \cdot 10^{-1}$ | $b_{72} = 0.5915308 \cdot 10^{-1}$ | |

Table A.3: *Coefficients for calculating the isothermal compressibility factor for methane.*

# Appendix B

# Ternary Mixture Models

## B.1 CO2-CH4-C9H20

Range:
$230K \leq T \leq 320K$
$5bar \leq p \leq 45bar$
$0.00 \leq y^{eq}_{CO_2} \leq 0.03$

Model:

$$x^{eq}_{CO_2} = y^{eq}_{CO_2} \left[ x^{CO_2}_0(p) + x^{CO_2}_1(p) \exp \left( -\frac{T}{x^{CO_2}_2(p)} \right) \right] \tag{B.1}$$

$$\begin{aligned} x^{eq}_{C_9} = x^{C_9}_0(p) + x^{C_9}_1(p) \exp \left( -\frac{T}{x^{C_9}_2(p)} \right) + \\ + y^{eq}_{CO_2} \left[ x^{C_9}_3(p) + x^{C_9}_4(p) \exp \left( -\frac{T}{x^{C_9}_5(p)} \right) \right] \end{aligned} \tag{B.2}$$

$$x^{eq}_{C_1} = 1 - (x^{eq}_{CO_2} + x^{eq}_{C_9}) \tag{B.3}$$

$$y^{eq}_{C_9} = y^{C_9}_0(p) \exp(y^{C_9}_1(p) + y^{C_9}_2(p)T + y^{C_9}_3(p)T^2) \tag{B.4}$$

$$y^{eq}_{C_1} = 1 - (y^{eq}_{CO_2} + y^{eq}_{C_9}) \tag{B.5}$$

$$x^{CO_2}_0(p) = 8.33 \cdot 10^{-1} - 8.34 \cdot 10^{-1} \exp \left( -\frac{p}{85.99} \right) \tag{B.6}$$

$$x^{CO_2}_1(p) = 1.099 + 55.18p - 1.141p^2 + 4.63 \cdot 10^{-3}p^3 \tag{B.7}$$

$$x^{CO_2}_2(p) = 31.58 + 9.64 \cdot 10^{-1} \exp \left( \frac{p}{25.35} \right) \tag{B.8}$$

$$x^{C_9}_0(p) = 1 - 3.52 \cdot 10^{-3}p + 7.11 \cdot 10^{-6}p^2 \tag{B.9}$$

69

$$x_1^{C_9}(p) = -17.36 + 18.04 \exp\left(-\frac{p}{24.77}\right) \tag{B.10}$$

$$x_2^{C_9}(p) = 47.12 + 1.142 \exp\left(\frac{p}{34.01}\right) \tag{B.11}$$

$$x_3^{C_9}(p) = -3.256 \cdot 10^{-1} + 3.273 \cdot 10^{-1} \exp\left(-\frac{p}{60.67}\right) \tag{B.12}$$

$$x_4^{C_9}(p) = -8.187 - 47.68p + 1.039p^2 - 5.83 \cdot 10^{-3}p^3 \tag{B.13}$$

$$x_5^{C_9}(p) = 30.08 + 2.493 \exp\left(\frac{p}{43.67}\right) \tag{B.14}$$

$$y_0^{C_9}(p) = \begin{array}{ll} 1.761 - 1.912 \cdot 10^{-1}p + 1.497 \cdot 10^{-2}p^2 - & 230 \leq T \leq 270 \\ -5.188 \cdot 10^{-4}p^3 + 8.505 \cdot 10^{-6}p^4 - 5.526 \cdot 10^{-8}p^5 & \\ 1.773 - 1.934 \cdot 10^{-1}p + 1.509 \cdot 10^{-2}p^2 - & 270 < T \leq 320 \\ -5.221 \cdot 10^{-4}p^3 + 8.579 \cdot 10^{-6}p^4 - 5.597 \cdot 10^{-8}p^5 & \end{array} \tag{B.15}$$

$$y_1^{C_9}(p) = \begin{array}{ll} -61.45 + 1.364 \cdot 10^{-1}p + 8.90 \cdot 10^{-3}p^2, & 230 \leq T \leq 270 \\ -48.65 + 1.387 \cdot 10^{-1}p + 2.85 \cdot 10^{-3}p^2, & 270 < T \leq 320 \end{array} \tag{B.16}$$

$$y_2^{C_9}(p) = \begin{array}{ll} 3.151 \cdot 10^{-1} - 1.18 \cdot 10^{-3}p - 5.524 \cdot 10^{-5}p^2, & 230 \leq T \leq 270 \\ 2.202 \cdot 10^{-1} - 1.21 \cdot 10^{-3}p - 9.745 \cdot 10^{-6}p^2, & 270 < T \leq 320 \end{array} \tag{B.17}$$

$$y_3^{C_9}(p) = \begin{array}{ll} -4.387 \cdot 10^{-4} + 1.467 \cdot 10^{-6}p + 1.012 \cdot 10^{-7}p^2, & 230 \leq T \leq 270 \\ -2.629 \cdot 10^{-4} + 1.565 \cdot 10^{-6}p + 1.516 \cdot 10^{-8}p^2, & 270 < T \leq 320 \end{array} \tag{B.18}$$

## B.2   CH4-C3H8-C9H20

Range:
$225K \leq T \leq 245K$
$6bar \leq p \leq 14bar$
$0.00 \leq y_{C_3}^{eq} \leq 0.02$

Model:

$$x_{C_3}^{eq} = y_{C_3}^{eq} \left[ x_0^{C_3}(p) + x_1^{C_3}(p) \exp\left(-\frac{T}{x_2^{C_3}(p)}\right) \right] + \\ + \left(y_{C_3}^{eq}\right)^2 \left[ x_3^{C_3}(p) + x_4^{C_3}(p) \exp\left(-\frac{T}{x_2^{C_3}(p)}\right) \right] \tag{B.19}$$

$$x_{C_9}^{eq} = x_0^{C_9}(p) + x_1^{C_9}(p) \exp\left(-\frac{T}{x_2^{C_9}(p)}\right) +$$

$$+ y_{C_3}^{eq}\left[x_3^{C_9}(p) + x_4^{C_9}(p) \exp\left(-\frac{T}{x_5^{C_9}(p)}\right)\right] +$$

$$+ \left(y_{C_3}^{eq}\right)^2\left[x_6^{C_9}(p) + x_7^{C_9}(p) \exp\left(-\frac{T}{x_8^{C_9}(p)}\right)\right] \tag{B.20}$$

$$x_{C_1}^{eq} = 1 - (x_{C_3}^{eq} + x_{C_9}^{eq}) \tag{B.21}$$

$$y_{C_9}^{eq} = \exp(y_0^{C_9}(p) + y_1^{C_9}(p)T + y_2^{C_9}(p)T^2) +$$

$$+ y_{C_3}^{eq}\left[\exp(y_3^{C_9}(p) + y_4^{C_9}(p)T + y_5^{C_9}(p)T^2)\right] \tag{B.22}$$

$$y_{C_1}^{eq} = 1 - (y_{C_3}^{eq} + y_{C_9}^{eq}) \tag{B.23}$$

$$x_0^{C_3}(p) = 4.46 - 4.546 \exp\left(-\frac{p}{19.68}\right) \tag{B.24}$$

$$x_1^{C_3}(p) = 4.475 \cdot 10^4 + 2.799 \cdot 10^5 p - 1.865 \cdot 10^4 p^2 + 3.539 \cdot 10^2 p^3 \tag{B.25}$$

$$x_2^{C_3}(p) = 16.72 + 1.749 \exp\left(\frac{p}{24.45}\right) \tag{B.26}$$

$$x_3^{C_3}(p) = 5.172 - 4.547 \exp\left(\frac{p}{21.52}\right) \tag{B.27}$$

$$x_4^{C_3}(p) = 1.447 \cdot 10^{11} - 6.413 \cdot 10^{10} p + 3.36 \cdot 10^9 p^2 - 4.096 \cdot 10^7 p^3 \tag{B.28}$$

$$x_5^{C_3}(p) = 9.091 + 5.886 \cdot 10^{-1} \exp\left(\frac{p}{19.33}\right) \tag{B.29}$$

$$x_0^{C_9}(p) = 5.464 \cdot 10^{-1} - 4.545 \cdot 10^{-1} \exp\left(-\frac{p}{1.074 \cdot 10^2}\right) \tag{B.30}$$

$$x_1^{C_9}(p) = 3.488 - 2.533p + 1.665 \cdot 10^{-1} p^2 - 5.6 \cdot 10^{-3} p^3 \tag{B.31}$$

$$x_2^{C_9}(p) = 40.90 + 2.383 \cdot 10^{-2} \exp\left(\frac{p}{5.174}\right) \tag{B.32}$$

$$x_3^{C_9}(p) = -4.229 + 4.283 \exp\left(-\frac{p}{18.97}\right) \tag{B.33}$$

$$x_4^{C_9}(p) = -6.491 \cdot 10^4 - 2.767 \cdot 10^5 p + 1.866 \cdot 10^4 p^2 - 3.581 \cdot 10^2 p^3 \tag{B.34}$$

$$x_5^{C_9}(p) = 16.43 + 2.012 \exp\left(\frac{p}{26.37}\right) \tag{B.35}$$

$$x_6^{C_9}(p) = -7.445 + 6.764 \exp\left(\frac{p}{29.74}\right) \tag{B.36}$$

$$x_7^{C_9}(p) = -1.620 \cdot 10^{11} + 7.217 \cdot 10^{10} p - 4.408 \cdot 10^9 p^2 + 6.612 \cdot 10^7 p^3 \tag{B.37}$$

$$x_8^{C_9}(p) = 9.268 + 4.038 \cdot 10^{-1} \exp\left(\frac{p}{13.65}\right) \tag{B.38}$$

$$y_0^{C_9} = -67.02 + 2.026 \cdot 10^{-1}p + 1.073 \cdot 10^{-2}p^2 \tag{B.39}$$

$$y_1^{C_9} = 3.652 \cdot 10^{-1} - 2.49 \cdot 10^{-3}p - 3.786 \cdot 10^{-5}p^2 \tag{B.40}$$

$$y_2^{C_9} = -5.414 \cdot 10^{-4} + 3.828 \cdot 10^{-6}p + 8.079 \cdot 10^{-8}p^2 \tag{B.41}$$

$$y_3^{C_9} = -44.90 + 3.054 \cdot 10^{-1}p + 7.13 \cdot 10^{-3}p^2 \tag{B.42}$$

$$y_4^{C_9} = 2.295 \cdot 10^{-1} - 1.64 \cdot 10^{-3}p - 5.958 \cdot 10^{-5}p^2 \tag{B.43}$$

$$y_5^{C_9} = -3.529 \cdot 10^{-4} + 2.178 \cdot 10^{-6}p + 1.252 \cdot 10^{-7}p^2 \tag{B.44}$$

$$\rho_{1,0}^{eq} = \frac{p^s}{k_B T} \tag{B.45}$$

$$\rho_{1,0} = S\rho_{1,0}^{eq} \tag{B.46}$$

$$\rho_{1,0}^{eq} = \frac{f_e p^s}{Z k_B T} \tag{B.47}$$

$$y_{C_9}^{eq} = y_{C_9}^{eq}(y_{CO_2}^{eq}, p, T) \tag{B.48}$$

$$S = \frac{y_v}{y_v^{eq}} \tag{B.49}$$

$$y_{C_9}^{eq} = y_{C_9}^{eq}(y_{C_3}^{eq}, p, T) \tag{B.50}$$

$$J_v = 0 \rightarrow E_{v+1}^{eq} = C_v^{eq}\left(\frac{\rho_v}{\rho_{v+1}}\right)^{eq} \tag{B.51}$$

$$\rho_v^{eq} = \rho_1^{eq} \exp\left(-\frac{\sigma a_0}{k_B T}n_v^{2/3}\right) \tag{B.52}$$

$$J = C_v\rho_v - E_{v+1}^{eq}\rho_{v+1} \tag{B.53}$$

$$J = J_0 \exp\left(-\frac{4}{27}\frac{\theta^3}{(\ln S)^2}\right) \tag{B.54}$$

$$J = \left[\sum_{n_v=1}^{\infty}\frac{1}{S^{n_v}\sum_{n_g=0}^{\infty}C_{v,g}^v\rho_{v,g}^{eq}}\right]^{-1} \tag{B.55}$$

# Appendix C

# Experimental Data

| $exp$ | $T_{sat}(K)$ | $P_{sat}(bar)$ | $Q_1(nl/min)$ | $Q_2(nl/min)$ | $Y_{C3} \cdot 10^3$ |
|---|---|---|---|---|---|
| 16$apr$03 001 | 290.68 | 28.01 | 0.5270 | 1.4170 | 10.1 |
| 16$apr$03 002 | 290.68 | 28.01 | 0.5900 | 1.3580 | 10.1 |
| 20$apr$04 002 | 290.67 | 28.01 | 0.6740 | 1.1530 | 10.1 |
| 20$apr$04 003 | 290.68 | 28.01 | 0.4680 | 1.4870 | 10.1 |
| 18$oct$04 002 | 290.66 | 29.99 | 0.1616 | 0.7631 | 10.1 |

Table C.1: *Experimental data on mixture preparation for the methane-propane-nonane mixture, series 1.*

| $exp$ | $y_{C3,sat}^{eq} \cdot 10^3$ | $y_{C9,sat}^{eq} \cdot 10^5$ | $y_{C3,mix} \cdot 10^3$ | $y_{C9,mix} \cdot 10^5$ |
|---|---|---|---|---|
| 16$apr$03 001 | 10.1 | 31.0 | 10.1 | 22.66 |
| 16$apr$03 002 | 10.1 | 31.0 | 10.1 | 21.67 |
| 20$apr$04 002 | 10.1 | 31.0 | 10.1 | 19.62 |
| 20$apr$04 003 | 10.1 | 31.0 | 10.1 | 23.64 |
| 18$oct$04 002 | 10.0 | 31.0 | 10.0 | 25.54 |

Table C.2: *Mixture composition for series 1 of experiments of the methane-propane-nonane mixture using RKS equation of state.*

| exp | $T_0(K)$ | $P_0(bar)$ | $T_{cond}(K)$ | $P_{cond}(bar)$ | $T_{growth}(K)$ | $P_{growth}(bar)$ |
|---|---|---|---|---|---|---|
| 16apr03 001 | 295.65 | 25.21 | 234.3 | 9.84 | 242.2 | 11.30 |
| 16apr03 002 | 295.55 | 25.20 | 234.3 | 9.84 | 241.8 | 11.23 |
| 20apr04 002 | 296.85 | 25.21 | 234.4 | 9.68 | 242.2 | 11.11 |
| 20apr04 003 | 296.25 | 25.22 | 234.5 | 9.79 | 242.3 | 11.23 |
| 18oct04 002 | 295.25 | 25.22 | 235.1 | 10.03 | 243.4 | 11.60 |

Table C.3: *Pressures and temperatures obtained from the pressure profiles of the nucleation experiments with the methane-propane-nonane mixture of series 1. Temperatures were calculated using the RKS equation of state.*

| exp | $y^{eq}_{C9,cond} \cdot 10^7$ | $growthrate(\mu m^2 ms^{-1})$ | $S_{C9,exp}$ | $J(m^{-3}s^{-1})$ |
|---|---|---|---|---|
| 16apr03 001 | 44.1 | $1.98 \cdot 10^{-2}$ | 51.4 | $3.77 \cdot 10^{15}$ |
| 16apr03 002 | 43.8 | $1.82 \cdot 10^{-2}$ | 49.2 | $1.80 \cdot 10^{15}$ |
| 20apr04 002 | 44.8 | $1.94 \cdot 10^{-2}$ | 43.8 | $1.65 \cdot 10^{15}$ |
| 20apr04 003 | 45.1 | $2.02 \cdot 10^{-2}$ | 52.4 | $4.78 \cdot 10^{15}$ |
| 18oct04 002 | 47.5 | $2.14 \cdot 10^{-2}$ | 53.8 | $2.38 \cdot 10^{15}$ |

Table C.4: *Results of the nucleation experiments performed with the methane-propane-nonane mixture, data of experimental series 1.*

| $exp$ | $T_{sat}(K)$ | $P_{sat}(bar)$ | $Q_1(nl/min)$ | $Q_2(nl/min)$ | $Y_{C3} \cdot 10^3$ |
|---|---|---|---|---|---|
| 06$jul$05 002 | 290.64 | 30.00 | 0.2629 | 1.2766 | 10.0 |
| 07$jul$05 001 | 290.64 | 30.00 | 0.4026 | 1.5692 | 10.0 |
| 07$jul$05 002 | 290.64 | 31.10 | 0.5269 | 1.7120 | 10.0 |
| 07$jul$05 003 | 290.64 | 30.00 | 0.5389 | 1.4781 | 10.0 |
| 08$jul$05 001 | 290.64 | 30.00 | 0.2921 | 1.7884 | 10.0 |
| 08$jul$05 002 | 290.64 | 30.00 | 0.2269 | 1.8550 | 10.0 |
| 08$jul$05 003 | 290.62 | 30.00 | 0.1593 | 1.9191 | 10.0 |
| 09$jul$05 001 | 290.63 | 30.00 | 0.0937 | 1.9956 | 10.0 |
| 09$jul$05 002 | 290.63 | 30.00 | 0.0000 | 2.0475 | 10.0 |
| 09$jul$05 003 | 290.63 | 30.00 | 0.0497 | 2.0623 | 10.0 |
| 10$jul$05 001 | 290.63 | 30.00 | 0.1423 | 1.9685 | 10.0 |
| 10$jul$05 002 | 290.63 | 30.00 | 0.1847 | 1.9191 | 10.0 |
| 10$jul$05 003 | 290.63 | 30.00 | 2.2264 | 1.8624 | 10.0 |
| 11$jul$05 001 | 290.63 | 30.00 | 0.3929 | 1.6972 | 10.0 |
| 11$jul$05 002 | 290.63 | 30.00 | 0.4558 | 1.6258 | 10.0 |
| 11$jul$05 003 | 290.63 | 30.00 | 0.4026 | 1.7342 | 10.0 |
| 12$jul$05 001 | 290.63 | 30.00 | 0.4026 | 1.6529 | 10.0 |
| 12$jul$05 002 | 290.63 | 30.00 | 0.0000 | 2.1265 | 10.0 |
| 12$jul$05 003 | 290.63 | 30.00 | 0.0677 | 2.0673 | 10.0 |

Table C.5: *Experimental data on mixture preparation for the methane-propane-nonane mixture, series 2.*

| exp | $y^{eq}_{C3,sat} \cdot 10^3$ | $y^{eq}_{C9,sat} \cdot 10^5$ | $y_{C3,mix} \cdot 10^3$ | $y_{C9,mix} \cdot 10^5$ |
|---|---|---|---|---|
| 06$jul$05 002 | 9.99 | 30.9 | 9.99 | 25.6 |
| 07$jul$05 001 | 9.99 | 30.9 | 9.99 | 24.6 |
| 07$jul$05 002 | 10.0 | 31.0 | 10.0 | 23.7 |
| 07$jul$05 003 | 9.99 | 30.9 | 9.99 | 22.7 |
| 08$jul$05 001 | 9.99 | 30.9 | 9.99 | 26.6 |
| 08$jul$05 002 | 9.99 | 30.9 | 9.99 | 27.6 |
| 08$jul$05 003 | 9.99 | 30.9 | 9.99 | 28.5 |
| 09$jul$05 001 | 9.99 | 30.9 | 9.99 | 29.5 |
| 09$jul$05 002 | 9.99 | 30.9 | 9.99 | 30.9 |
| 09$jul$05 003 | 9.99 | 30.9 | 9.99 | 30.2 |
| 10$jul$05 001 | 9.99 | 30.9 | 9.99 | 28.8 |
| 10$jul$05 002 | 9.99 | 30.9 | 9.99 | 28.2 |
| 10$jul$05 003 | 9.99 | 30.9 | 9.99 | 27.4 |
| 11$jul$05 001 | 9.99 | 30.9 | 9.99 | 25.1 |
| 11$jul$05 002 | 9.99 | 30.9 | 9.99 | 24.1 |
| 11$jul$05 003 | 9.99 | 30.9 | 9.99 | 25.1 |
| 12$jul$05 001 | 9.99 | 30.9 | 9.99 | 24.9 |
| 12$jul$05 002 | 9.99 | 30.9 | 9.99 | 30.9 |
| 12$jul$05 003 | 9.99 | 30.9 | 9.99 | 29.9 |

Table C.6: *Mixture composition for series 2 of experiments of the methane-propane-nonane mixture using RKS equation of state.*

| exp | $T_0(K)$ | $P_0(bar)$ | $T_{cond}(K)$ | $P_{cond}(bar)$ | $T_{growth}(K)$ | $P_{growth}(bar)$ |
|---|---|---|---|---|---|---|
| 06$jul$05 002 | 294.45 | 24.80 | 236.0 | 10.12 | 243.6 | 11.56 |
| 07$jul$05 001 | 294.85 | 24.90 | 236.0 | 10.11 | 243.9 | 11.60 |
| 07$jul$05 002 | 294.55 | 24.78 | 236.1 | 10.12 | 243.7 | 11.55 |
| 07$jul$05 003 | 294.75 | 24.80 | 236.2 | 10.11 | 244.0 | 11.58 |
| 08$jul$05 001 | 294.65 | 24.85 | 236.1 | 10.14 | 243.8 | 11.60 |
| 08$jul$05 002 | 294.75 | 24.85 | 236.7 | 10.21 | 243.9 | 11.60 |
| 08$jul$05 003 | 294.65 | 24.85 | 235.8 | 10.09 | 243.8 | 11.60 |
| 09$jul$05 001 | 294.55 | 24.80 | 236.5 | 10.19 | 244.2 | 11.66 |
| 09$jul$05 002 | 294.85 | 24.85 | 236.1 | 10.11 | 244.2 | 11.63 |
| 09$jul$05 003 | 295.05 | 24.85 | 236.5 | 10.14 | 244.3 | 11.62 |
| 10$jul$05 001 | 294.85 | 24.85 | 236.7 | 10.20 | 244.3 | 11.66 |
| 10$jul$05 002 | 295.05 | 24.90 | 236.5 | 10.17 | 244.4 | 11.67 |
| 10$jul$05 003 | 295.25 | 24.97 | 236.5 | 10.16 | 244.3 | 11.65 |
| 11$jul$05 001 | 294.25 | 25.02 | 237.2 | 10.31 | 244.5 | 11.70 |
| 11$jul$05 002 | 294.05 | 25.05 | 234.7 | 10.07 | 242.8 | 11.60 |
| 11$jul$05 003 | 295.15 | 24.79 | 236.3 | 10.22 | 243.8 | 11.65 |
| 12$jul$05 001 | 295.25 | 25.02 | 236.3 | 10.16 | 244.4 | 11.68 |
| 12$jul$05 002 | 294.15 | 24.78 | 235.9 | 10.15 | 243.7 | 11.62 |
| 12$jul$05 003 | 194.15 | 24.74 | 236.3 | 10.19 | 243.4 | 11.55 |

Table C.7: *Pressures and temperatures obtained from the pressure profiles of the nucleation experiments with the methane-propane-nonane mixture of series 2. Temperatures were calculated using the RKS equation of state.*

| $exp$ | $y^{eq}_{C9,cond} \cdot 10^7$ | $growthrate(\mu m^2 ms^{-1})$ | $S_{C9,exp}$ | $J(m^{-3}s^{-1})$ |
|---|---|---|---|---|
| 06$jul$05 002 | 51.6 | $2.12 \cdot 10^{-2}$ | 49.5 | $7.83 \cdot 10^{15}$ |
| 07$jul$05 001 | 52.2 | $1.93 \cdot 10^{-2}$ | 47.2 | $3.13 \cdot 10^{15}$ |
| 07$jul$05 002 | 52.5 | $1.85 \cdot 10^{-2}$ | 45.1 | $1.12 \cdot 10^{15}$ |
| 07$jul$05 003 | 53.0 | $1.74 \cdot 10^{-2}$ | 42.7 | $3.05 \cdot 10^{14}$ |
| 08$jul$05 001 | 52.7 | $1.97 \cdot 10^{-2}$ | 50.4 | $5.10 \cdot 10^{15}$ |
| 08$jul$05 002 | 55.5 | $2.05 \cdot 10^{-2}$ | 49.6 | $5.46 \cdot 10^{15}$ |
| 08$jul$05 003 | 51.2 | $2.22 \cdot 10^{-2}$ | 55.8 | $2.35 \cdot 10^{16}$ |
| 09$jul$05 001 | 54.5 | $2.23 \cdot 10^{-2}$ | 54.2 | $2.15 \cdot 10^{16}$ |
| 09$jul$05 002 | 52.7 | $2.33 \cdot 10^{-2}$ | 58.7 | $6.45 \cdot 10^{16}$ |
| 09$jul$05 003 | 54.9 | $2.10 \cdot 10^{-2}$ | 55.0 | $2.98 \cdot 10^{16}$ |
| 10$jul$05 001 | 55.7 | $2.21 \cdot 10^{-2}$ | 51.7 | $7.70 \cdot 10^{15}$ |
| 10$jul$05 002 | 54.8 | $2.02 \cdot 10^{-2}$ | 51.4 | $4.03 \cdot 10^{15}$ |
| 10$jul$05 003 | 54.5 | $1.98 \cdot 10^{-2}$ | 50.3 | $3.97 \cdot 10^{15}$ |
| 11$jul$05 001 | 58.6 | $1.87 \cdot 10^{-2}$ | 42.9 | $3.62 \cdot 10^{14}$ |
| 11$jul$05 002 | 45.4 | $1.75 \cdot 10^{-2}$ | 53.2 | $2.94 \cdot 10^{15}$ |
| 11$jul$05 003 | 53.3 | $1.86 \cdot 10^{-2}$ | 47.0 | $8.20 \cdot 10^{14}$ |
| 12$jul$05 001 | 53.7 | $1.79 \cdot 10^{-2}$ | 46.3 | $3.75 \cdot 10^{14}$ |
| 12$jul$05 002 | 51.6 | $2.31 \cdot 10^{-2}$ | 59.9 | $5.70 \cdot 10^{16}$ |
| 12$jul$05 003 | 53.3 | $2.36 \cdot 10^{-2}$ | 56.1 | $2.77 \cdot 10^{16}$ |

Table C.8: *Results of the nucleation experiments performed with the methane-propane-nonane mixture, data of experimental series 2.*

# Appendix D

# Correction of Experimental Series April 2005

In April 2005 another series of experiments was conducted with the ternary methane-propane-nonane mixture. In these experiments, nucleation of the ternary methane-propane-n-nonane mixture was studied at nucleation conditions of approximately $235\,K$, $10\,bar$ and a propane fraction around 1%. In these series of experiments, something went wrong with the mixture preparation, leading to inaccurate values of the nonane vapour fraction $y_{C9,mix}$. Droplet growth rates, nucleation rates, pressures and temperatures of the experiments are known and can be found in Table D.1 and Table D.2.

In an attempt to obtain values for the nonane vapour fraction, the principle of the same correction is followed as in the results chapter for the other experimental series. As droplet

| $exp$ | $T_0(K)$ | $P_0(bar)$ | $T_{cond}(K)$ | $P_{cond}(bar)$ | $T_{growth}(K)$ | $P_{growth}(bar)$ |
|---|---|---|---|---|---|---|
| 13apr05 002 | 294.85 | 25.09 | 234.8 | 9.99 | 242.8 | 11.48 |
| 13apr05 003 | 294.95 | 25.14 | 234.6 | 9.95 | 242.8 | 11.49 |
| 14apr05 001 | 295.15 | 25.03 | 235.2 | 9.98 | 243.2 | 11.48 |
| 14apr05 002 | 294.85 | 25.08 | 235.4 | 10.08 | 243.2 | 11.56 |
| 15apr05 002 | 294.75 | 24.74 | 235.6 | 9.99 | 243.8 | 11.52 |
| 20apr05 001 | 294.75 | 25.04 | 235.5 | 10.09 | 243.3 | 11.58 |
| 20apr05 002 | 295.25 | 25.20 | 235.2 | 10.03 | 243.1 | 11.53 |
| 21apr05 001 | 294.85 | 25.09 | 235.3 | 10.06 | 243.1 | 11.55 |
| 22apr05 001 | 295.05 | 25.09 | 235.6 | 10.10 | 243.4 | 11.57 |
| 22apr05 002 | 295.05 | 25.14 | 235.4 | 10.08 | 243.0 | 11.52 |

Table D.1: *Pressures and temperatures obtained from the pressure profiles of the nucleation experiments with the methane-propane-nonane mixture of the series of experiments from April 2005. Temperatures were calculated using the RKS equation of state.*

| $exp$ | $y^{eq}_{C9,cond} \cdot 10^7$ | $growthrate(\mu m^2 ms^{-1})$ | $S_{C9,exp}$ | $J(m^{-3}s^{-1})$ | $y_{C9,mix} \cdot 10^5$ |
|---|---|---|---|---|---|
| 13apr05 002 | 46.3 | $1.85 \cdot 10^{-2}$ | 49.1* | $1.43 \cdot 10^{15}$ | 22.7* |
| 13apr05 003 | 45.1 | $2.02 \cdot 10^{-2}$ | 54.8* | $8.05 \cdot 10^{15}$ | 24.7* |
| 14apr05 001 | 48.1 | $1.89 \cdot 10^{-2}$ | 48.3* | $3.19 \cdot 10^{15}$ | 23.2* |
| 14apr05 002 | 48.8 | $2.23 \cdot 10^{-2}$ | 55.7* | $1.59 \cdot 10^{16}$ | 27.2* |
| 15apr05 002 | 50.4 | $2.17 \cdot 10^{-2}$ | 56.6* | $1.93 \cdot 10^{16}$ | 26.5* |
| 20apr05 001 | 49.4 | $1.81 \cdot 10^{-2}$ | 45.2* | $4.72 \cdot 10^{14}$ | 22.3* |
| 20apr05 002 | 47.9 | $1.84 \cdot 10^{-2}$ | 47.3* | $7.96 \cdot 10^{14}$ | 22.7* |
| 21apr05 001 | 48.3 | $1.78 \cdot 10^{-2}$ | 45.3* | $3.21 \cdot 10^{14}$ | 21.9* |
| 22apr05 001 | 50.2 | $1.86 \cdot 10^{-2}$ | 45.5* | $7.43 \cdot 10^{14}$ | 22.8* |
| 22apr05 002 | 49.2 | $1.99 \cdot 10^{-2}$ | 49.6* | $3.71 \cdot 10^{15}$ | 24.4* |

Table D.2: *Results of the nucleation experiments performed with the methane-propane-nonane mixture, data of the experimental series in April 2005. Data with a * are corrected data using the average diffusion coefficient of series 1 and 3.*

growth temperatures and pressures as well as propane gas fractions of the April 2005 series are comparable to both valid experimental series 1 and 2, the average diffusion coefficient is taken of both series to correct for the April 2005 series. This way corresponding values for the nonane vapour fraction can be found for each experiment, and thus leading to corrected values for supersaturation values, these corrected values can be found in Table D.2. The nucleation rate curve for all three series with the corrected supersaturation values for series April 2005 is displayed in Fig. D.1.

As can be seen in this figure, the corrected results of the April 2005 series align well with the other series of experiments and thus support the overall nucleation results.
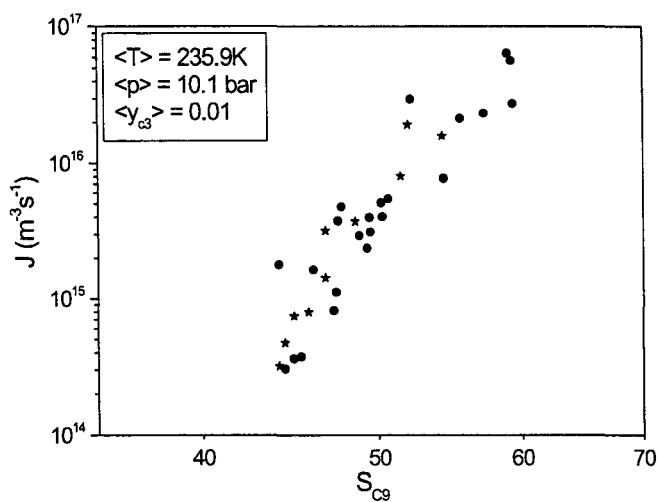
Figure D.1: *Nucleation rate versus supersaturation for nucleation experiments of the methane-propane-nonane mixture, the propane vapour fraction is approximately 1%. Circles are experimental results for series 1 and 3, the nonane vapour fraction is corrected by the average diffusion coefficient of each series. Stars are experimental results of the April 2005 series, nonane vapour fractions are corrected using the average value of the average diffusion coefficients of series 1 and 3. The supersaturation is temperature corrected to the average temperature of the experiments of series 1 and 3.*